ISTANBUL TECHNICAL UNIVERSITY ★ GRADUATE SCHOOL OF SCIENCE ENGINEERING AND TECHNOLOGY

PREPARATION OF TRANSPARENT CONDUCTIVE ELECTRODES VIA LAYER BY LAYER DEPOSITION OF FUNCTIONAL NANOMATERIALS

Ph.D. THESIS

Faruk OYTUN

Department of Chemistry

Chemistry Programme

JULY 2019

ISTANBUL TECHNICAL UNIVERSITY ★ GRADUATE SCHOOL OF SCIENCE ENGINEERING AND TECHNOLOGY

PREPARATION OF TRANSPARENT CONDUCTIVE ELECTRODES VIA LAYER BY LAYER DEPOSITION OF FUNCTIONAL NANOMATERIALS

Ph.D. THESIS

Faruk OYTUN
(509122016)

Department of Chemistry

Chemistry Programme

Thesis Advisor: Asst. Prof. Dr. Onur ALPTÜRK
Thesis Co-Advisor: Assoc. Prof. Dr. Fevzihan BAŞARIR

JULY 2019

İSTANBUL TEKNİK ÜNİVERSİTESİ ★ FEN BİLİMLERİ ENSTİTÜSÜ

FONKSİYONEL NANOMALZEMELERİN KATMAN KATMAN KAPLANMASI İLE SAYDAM İLETKEN ELEKTROTLARIN HAZIRLANMASI

DOKTORA TEZİ

Faruk OYTUN
(509122016)

Kimya Anabilim Dalı

Kimya Programı

Tez Danışmanı: Dr. Öğr. Üyesi Onur ALPTÜRK
Eş Danışman: Doç. Dr. Fevzihan BAŞARIR

TEMMUZ 2019

Faruk Oytun, a Ph.D. student of ITU Graduate School of Science Engineering and Technology student ID 509122016, successfully defended the thesis entitled "PREPARATION OF TRANSPARENT CONDUCTIVE ELECTRODES VIA LAYER BY LAYER DEPOSITION OF FUNCTIONAL NANOMATERIALS", which he prepared after fulfilling the requirements specified in the associated legislations, before the jury whose signatures are below.

Thesis Advisor:	**Asst. Prof. Dr. Onur ALPTÜRK** Istanbul Technical University	.....
Co-advisor:	**Assoc. Prof.Dr. Fevzihan BAŞARIR** TUBITAK	.....
Jury Members:	**Prof. Dr. Nilgün KARATEPE YAVUZ** Istanbul Technical University	.....
	Prof. Dr. Mehmet Atilla TAŞDELEN Yalova University	.....
	Prof. Dr. Turan ÖZTÜRK Istanbul Technical University	.....
	Prof. Dr. Volkan GÜNAY Yeditepe University	.....
	Prof. Dr. İsmail AYDIN Istanbul University	.....

Date of Submission : 29 May 2019
Date of Defense : 10 July 2019

To my parents and my wife

FOREWORD

There are many people who have been helpful in a variety ways for the completion of this work. Foremost, I would like to express my sincere gratitude to my advisors Assist. Prof. Dr. Onur ALPTÜRK and Assoc. Prof. Dr. Fevzihan BAŞARIR for the continuous support of my Ph.D. study and research, for their patience, motivation, my enthusiasm, and immense knowledge. Their guidances helped me at all the time of research and writing of this thesis.

I would also like to thank Prof. Turan ÖZTÜRK, Prof. Volkan GÜNAY, Prof. İsmail AYDIN and Prof. Mehmet Atilla TAŞDELEN for serving on my guidance and dissertation committee.

I am grateful to Prof. Nilgun YAVUZ and Prof. Hyosung CHOI and their group members for their help.

My special thanks go out to: Çağatay ALTINKÖK, Mustafa ÇİFTÇİ, Umut Uğur ÖZKÖSE, Büşra Tuğba ÇAMİÇ, Cem BERK, Assoc. Prof. Muhammet KAHVECİ, Dr. Gökhan AÇIK, Dr. Cihat TAŞALTIN, Amin TABATABAEI, Farid Sayar IRANI and the countless others who have helped me along the way.

I owe special thanks to my old housemates Çağatay ALTINTAŞ, Burak YÜKSEL, Çağrı ÖZDEMİR, Onur YILDIZ and Fatih KAZALCI. We had some great times together and I will always remember it.

I also would like to specially thank to my brother-in-law Volkan AKTAŞ. He was always with me at every moment of my Ph.D. study and supported me enourmously.

I also would like to thank my mother and father. They have spent many nights praying for my success and have supported me throughout every step of my life and have always gone out of their way to help me.

Last but not the least, I would like to extend my sincere gratitude to my wife Gülay OYTUN for her unwavering support and inexhaustible tolerance during the Ph.D. work. Without her love, understanding and constant encouragement, I would never have come this far. Although I neglected her so much during my Ph.D., she has always been behind me.

July 2019

Faruk OYTUN
(M.Sc. Chemist)

TABLE OF CONTENTS

Page

ABBREVIATIONS

AFM	**:** Atomic Force Microscopy
AgNW	**:** Silver Nanowire
AgNW-COOH	**:** Carboxylic acid-functionalized Silver Nanowire
AgNW-NH_2	**:** Amine-functionalized Silver Nanowire
APTES	**:** Aminopropyltriethoxysilane
CA	**:** Cysteamine
CVD	**:** Chemical Vapor Deposition
DI	**:** Deionized Water
DMF	**:** Dimethyl Formamide
FE-SEM	**:** Field Emission Scanning Electron Microscope
FOM	**:** Figure of Merit
f-TFH	**:** Flexible Transparent Film Heater
FT-IR	**:** Fourier Transform Infrared Spectrometer
ITO	**:** Indium Tin Oxide
LBL	**:** Layer by Layer
LED	**:** Light Emitting Diode
MPA	**:** Mercaptopropionic acid
MTP	**:** Multilayer Transfer Printing
MWCNT	**:** Multi-walled Carbon Nanotube
MWCNT-COOH	**:** Carboxylic acid-functionalized Multi-walled Carbon Nanotube
MWCNT-NH_2	**:** Amine-functionalized Multi-walled Carbon Nanotube
OPV	**:** Organic Photovoltaic
PSU	**:** Polysulfone
PVP	**:** Poly vinylpyrolidone
SWCNT	**:** Single-walled Carbon Nanotube
SWCNT-COOH	**:** Carboxylic acid-functionalized Single-walled Carbon Nanotube
SWCNT-NH_2	**:** Amine-functionalized Single-walled Carbon Nanotube
TCE	**:** Transparent Conductive Electrode
XPS	**:** X-ray Photoelectron Spectrometer

LIST OF TABLES

Page

LIST OF FIGURES

Page

PREPARATION OF TRANSPARENT CONDUCTIVE ELECTRODES VIA LAYER BY LAYER DEPOSITION OF FUNCTIONAL NANOMATERIALS

SUMMARY

Transparent conductive electrodes are the key element of the various optoelectronic devices. Traditionally, indium tin oxide (ITO) has been utilized as transparent conductive electrode in the optoelectronic devices. However, ITO has some disadvantages. Because, limited supply of indium and increasing demand has increased the ITO price drastically since the past decades. In addition, high vacuum and temperature is needed for sputtering ITO on the substrate, which also increases the cost. Besides, the brittle nature of ITO causes device failure upon bending when it is used on flexible substrates. Therefore, there has been great research effort on development of ITO free transparent conductive electrodes. Up to date, researchers have utilized various materials such as conducting polymers, carbon nanotubes (CNTs), graphene and metallic nanowires. These materials have been widely utilized, owing to their promising and new technology. Meanwhile, they have demonstrated remarkable mechanical, thermal, optical, electrochemical and electrical properties, which allowed them to be utilized in many new applications. Thus, various methods have been developed to prepare transparent conductive electrode with nanomaterials; such as brush painting, spray coating, vacuum filtration and rod/wire coating. The aforementioned methods are considered as the most simple and flexible method, but the films obtained generally have sparse density, which led to high sheet resistance and poor device performance. These methods have also common drawbacks such as reproducibility, and poor adhesion of the nanomaterials to the substrate. On the other hand, layer-by-layer (LBL) deposition consisting of sequential immersion of a substrate into aqueous solutions of oppositely charged materials is a very promising approach. This method can create versatile thin films with highly tunable thickness, porosity, packing density and surface properties. In addition, the adhesion of the multilayer film to the substrate is very good since the multilayer is formed via covalent bonding or ionic interaction. Thus, it has been widely utilized for using in various electronic and electrochemical applications.

Taking account of the unique advantages of LBL deposition, in this thesis, we focused on the preparation of transparent conductive electrodes using functional nanomaterials.

In the first part of the thesis, transparent conducting electrodes were prepared on flexible polysulfone (PSU) film via multilayer transfer of multi-walled carbon nanotubes (MWCNTs) and single-walled carbon nanotubes (SWCNTs) coated on glass substrates via LBL deposition. First, bare CNTs were functionalized with carboxylic acid and amine moieties to obtain negatively and positively charged nanotubes, respectively (Figure 1). Then, functionalized CNTs were coated sequentially on glass substrate via LBL deposition, which was followed by subjecting the multilayer to various chemical and thermal post-treatment processes to improve the electrical conductivity. Next, the multilayer was transferred from the glass substrate to polymer film by coating and detaching the PSU film. The highest

figure of merit was found to be 2.52×10^{-6} Ω^{-1} at 68% optical transmission and 1.14×10^{-3} Ω^{-1} at 81% optical transmission for MWCNT and SWCNT films, respectively. Finally, the use of transparent electrode was demonstrated in resistive touch sensor.

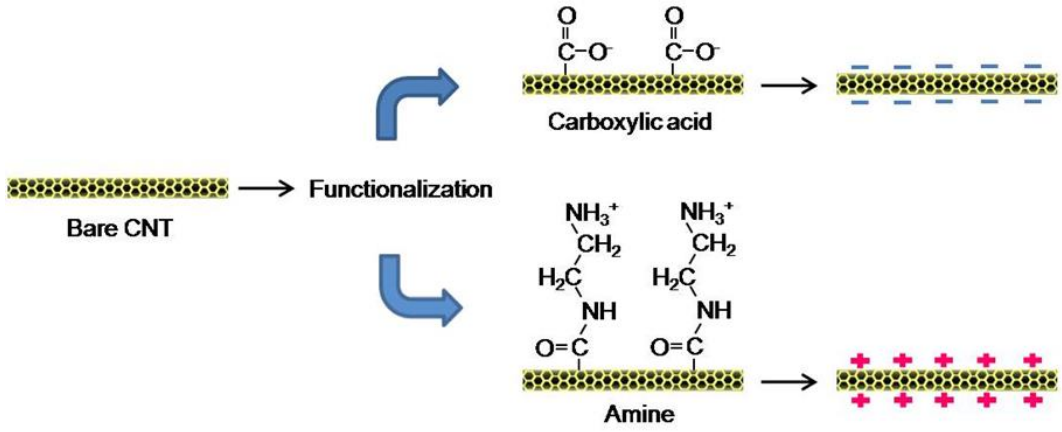

Figure 1 : Chemical functionalization of carbon nanotubes.

In the second part, highly transparent and conductive silver nanowire (AgNW) electrodes on glass substrates were prepared via LBL deposition of functionalized AgNWs (Figure 2). First, commercial AgNWs were functionalized with cysteamine hydrochloride (CA) and 3-mercaptopropionic acid (MPA) to obtain positively and negatively charged AgNWs, respectively. Then, oppositely charged AgNWs were coated sequentially on 3-aminopropyltriethoxysilane (APTES) modified glass substrate via LBL deposition, which provided highly controllable thin films in terms of optical transmittance and sheet resistance. Next, thermal annealing was performed to improve the electrical conductivity of the nanowire films. Finally, AgNW multilayer was characterized by UV–Vis spectrometer, field emission scanning electron microscope (FE-SEM), optical microscope (OM) and sheet resistance measurement by four-point probe method. The best result was achieved with 6-bilayer film which provided a sheet resistance of 18.3 Ω/□ with an optical transmittance of 83.8% at 550 nm, which is comparable to commercial ITO electrode.

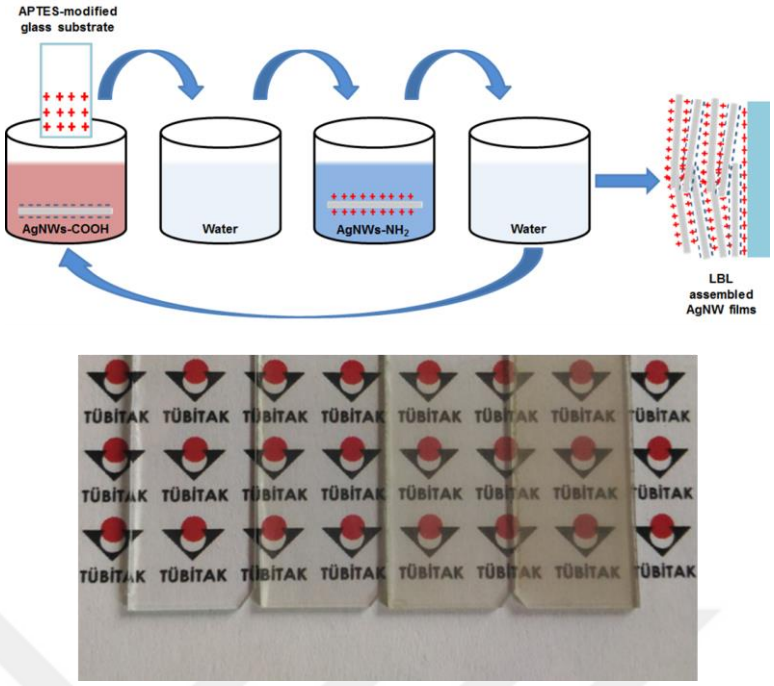

Figure 2 : Preparation of transparent conductive AgNW films via LBL.

Finally, flexible transparent film heaters (f-TFH) were prepared on a PSU film with a multilayer transfer of AgNWs coated on glass substrates via LBL deposition (Figure 3). First, as-received AgNWs were functionalized with carboxylic acid (AgNW-COOH) and amine (AgNW-NH_2) moieties to obtain negatively and positively charged nanowires, respectively. Second, functionalized AgNWs were sequentially coated on a glass substrate via the LBL deposition, which was followed by subjecting the multilayer film to annealing at 125 °C for 30 min to improve the electrical conductivity. Third, the multilayer was transferred from the glass substrate to the polymer film by coating and detaching the PSU. The multilayer film provided optical transmission of 84% and sheet resistance of 12 Ω/□ with 5 bilayer sample, which is comparable to ITO film. The f-TFH reached maximum temperature of 128 °C at 7 V with a response time of 45 s. Moreover, it exhibited good defrosting capability by applying 7 V for 20 s. Cyclic bending test results indicated that the sheet resistance of the flexible multilayer film does not demonstrate any change until 300 cycles, while adhesion test 3-M tapes exhibited no sheet resistance change even after 20 peel cycles showing the superior performance of the multilayer film. In addition, the film showed stable heating performance at 128 °C for 5 h.

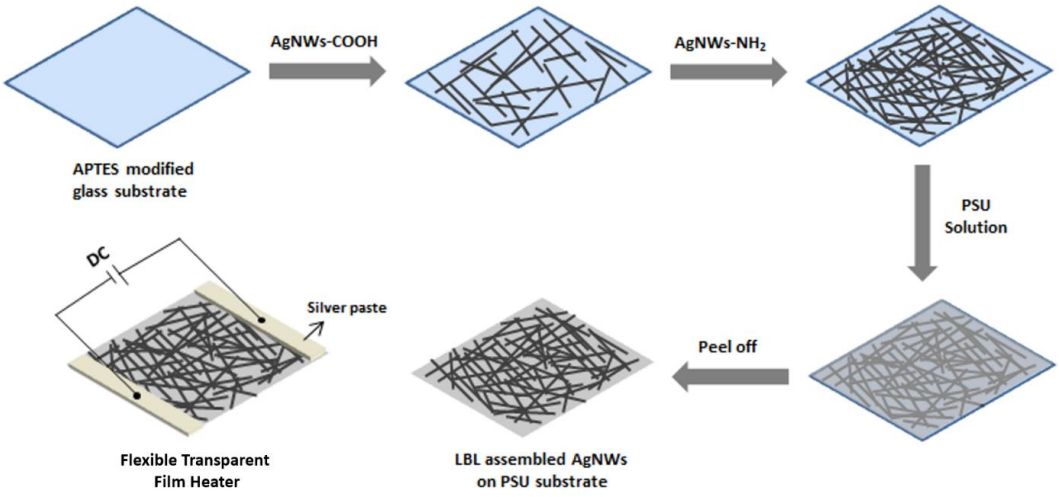

Figure 3 : Preparation of flexible AgNW transparent film heaters.

FONKSİYONEL NANOMALZEMELERİN KATMAN KATMAN KAPLANMASI İLE SAYDAM İLETKEN ELEKTROTLARIN HAZIRLANMASI

ÖZET

Saydam iletken elektrotlar, optoelektronik cihazların en önemli unsurlarından biridir. İndiyum kalay oksit geleneksel olarak optoelektronik cihazlarda en çok kullanılan malzemedir. Fakat bu malzeme bazı dezavantajlara sahiptir. Artan taleplere nazaran indiyum kaynaklarının gittikçe azalması indiyum kalay oksitin son zamanlarda fiyatının oldukça yükselmesine neden olmuştur. İndiyum kalay oksit üretiminde kullanılan yüksek vakum ve sıcaklık ekstra maliyet açısından farklı bir olumsuz yönü olarak bahsedilebilir. Tüm bunlara ek olarak, indiyum kalay oksitin kolay kırılabilir olması onun esnek uygulamalarda kullanımını zorlaştırır.

Bu yüzden, indiyum kalay oksitin alternatiflerini bulmak için pek çok araştırma yapılmıştır. Günümüze kadar, araştırmacılar iletken polimerler, karbon nanotüpler, grafen ve metalik nanoteller gibi çeşitli malzemeleri kullanmışlardır. Araştırma sonuçlarına göre bu malzemeler önemli derecede mekanik, ısısal, optik, elektrokimyasal ve elektriksel özellikler göstermiştir.

Bu malzemelerin kullanılmasıyla elde edilen saydam iletken elektrotlar genellikle fırça ile boyama, sprey kaplama, vakum süzme ve çubukla kaplama metotları kullanılarak elde edilmiştir. Bu metotlar oldukça basit ve kullanışlı bir metod olmasına rağmen, elde edilen filmler homojen olmamakla birlikte yüksek tabaka direncine ve kötü performansa sahip olduğu bulunmuştur. Bu metotların diğer dezavantajları ise tekrarlanabilirliğinin zor olması ve malzeme ile altlık arasındaki kötü yapışmaya neden olmasıdır.

Öte yandan, katman katman kaplama metodu zıt yüklü malzemelerin ardışık olarak kaplanması sonucu elde edilen çok umut verici bir yaklaşımdır. Bu metod ile kaplama kalınlıkları, gözenek kontrolü ve yüzey özellikleri kolayca ayarlanabilir. Ek olarak, kaplanan malzemeyle altlık arasındaki kovalent veya iyonik etkileşimlerden dolayı elde edilen filmlerdeki malzeme adezyonu oldukça iyidir. Bu durum, yaklaşımın çeşitli elektronik ve elektrokimyasal uygulamalarda kullanılabileceğini göstermektedir.

Bu tezde, katman katman kaplama metodunun tüm bu avantajları dikkate alınarak, fonksiyonel nanomalzemeler katman katman kaplama metodu kullanılarak saydam iletken elektrotların hazırlanması üzerine odaklanılmıştır.

Bu kapsamda tezin ilk bölümünde, saydam iletken elektrotlar; cam altlık üzerinde katman katman kaplanan çok duvarlı ve tek duvarlı karbon nanotüplerin esnek polisülfon altlık üzerine aktarılmasıyla hazırlanmıştır. Önce, karbon nanotüpler negatif ve pozitif yüklü karbon nanotüpler elde etmek için karboksilik asit ve amin gruplarıyla fonksiyonlandırıldı (Şekil 1). Sonra, fonksiyonlanan nanotüpler katman katman kaplama metoduyla cam altlık üzerine kaplanıp, sonrasında elektriksel iletkenliklerinin artması için kimyasal ve ısısal işlemlere maruz bırakılmıştır. Elde edilen filmler cam altlık üzerinden polisülfon altlık üzerine aktarılmıştır. Elde edilen en yüksek performans katsayısı çok duvarlı karbon nanotüp filmler için % 68 optik geçirgenlikte 2.52×10^{-6} Ω^{-1}, tek duvarlı karbon nanotop filmler için % 81 optik

geçirgenlikte 1.14×10^{-3} Ω^{-1} olarak bulunmuştur. Son olarak elde edilen esnek filmlerin dokunmatik sensör uygulamalarında kullanılabileceği gösterilmiştir.

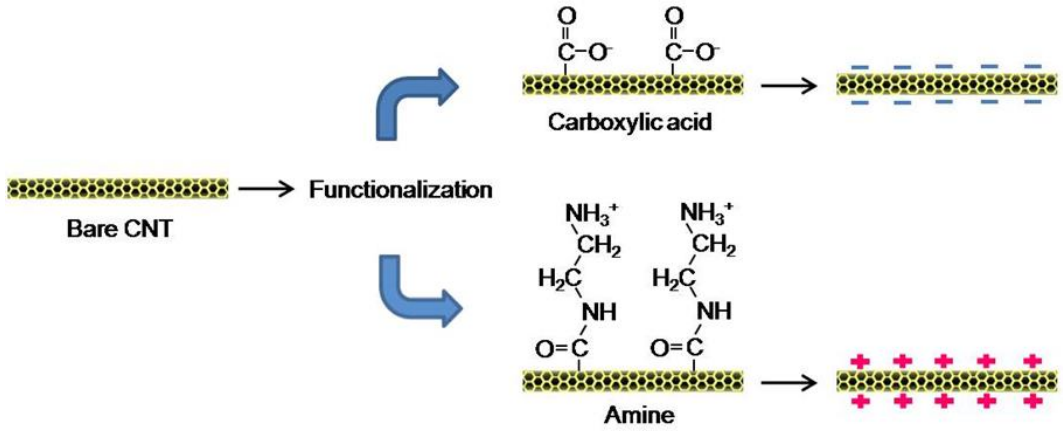

Şekil 1 : Karbon nanotüplerin kimyasal olarak fonksiyonlandırılması.

İkinci kısımda ise, yüksek saydamlık ve iletkenliğe sahip olan elektrotlar cam altlık üzerinde fonksiyonlandırılmış olan gümüş nanotellerin katman katman kaplanmasıyla hazırlanmıştır (Şekil 2). Önce, gümüş nanoteller negatif ve pozitif yüklü nanoteller elde etmek için karboksilik asit ve amin gruplarıyla kimyasal olarak fonksiyonlandırıldı. Zıt yük ile yüklenmiş olan bu gümüş nanoteller, aminopropil trietoksisilan ile modifiye edilmiş cam üzerine katman katman kaplanmıştır. Bu yöntemle kontrollü bir optik geçirgenlik ve elektriksel iletkenlik elde edilmiştir. Elde edilen filmler ısısal işleme tutulup elektriksel iletkenliklerinin artması sağlanmıştır. Son olarak elde edilen gümüş nanotel ince filmlerin karakterizasyonları yapılmıştır. En iyi film özelliklerine sahip olan 6 katman kaplanan film % 83.8 optik geçirgenlikte, 18.3 Ω/□ tabaka direnci göstermiştir. Bu sonuçlara göre elde edilen gümüş nanotel filmlerin ticari olarak kullanılan indiyum kalay oksit filmlere alternatif olabileceği gösterilmiştir.

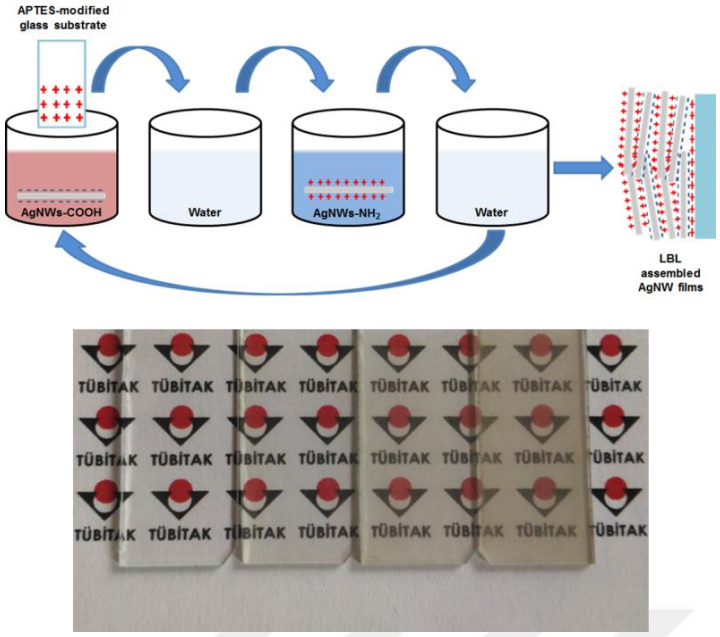

Şekil 2 : Katman katman kaplama metoduyla hazırlanan gümüş nanotellerde hazırlanan saydam iletken elektrotların hazırlanması.

Son olarak, esnek saydam film ısıtıcılar cam altlık üzerinde katman katman kaplanan gümüş nanotellerin esnek polisülfon altlık üzerine aktarılmasıyla hazırlanmıştır (Şekil 3). Önce, gümüş nanoteller negatif ve pozitif yüklü nanoteller elde etmek için karboksilik asit ve amin gruplarıyla fonksiyonlandırıldı. Sonra, fonksiyonlanan nanotüpler katman katman kaplama metoduyla cam altlık üzerine kaplanıp, sonrasında elektriksel iletkenliklerinin artması için 125 °C'de 30 dakika boyunca tavlanmıştır. Sonra, elde edilen filmler cam altlık üzerinden polisülfon altlık üzerine aktarılmıştır. En iyi film özelliklerine sahip olan 5 katman kaplanan film % 84 optik geçirgenlikte, 12 Ω/□ tabaka direnci göstermiştir. Elde edilen esnek filmlere 7 V'luk gerilim uygulandığında 128 °C'ye ulaştığı görülmüştür. Sıcaklığın sabit olana kadar geçen süre ise 45 saniye olarak bulunmuştur. Ayrıca elde edilen filmlerin yüksek mekanik özelliklere sahip olduğu gözlemlenmiştir.

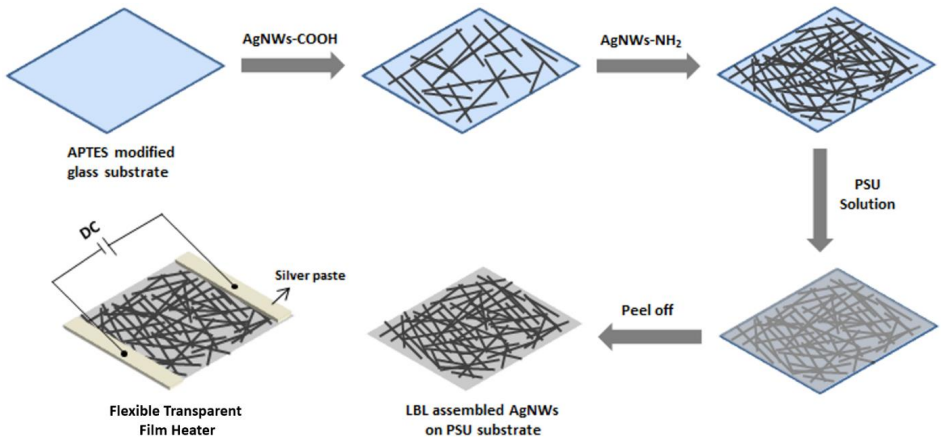

Şekil 3 : Gümüş nanotelden hazırlanan esnek saydam film ısıtıcılarının hazırlanması.

1. INTRODUCTION

Transparent conductive electrodes (TCEs), which transmit light and conduct electrical current simultaneously, are important components for many electronic devices, including liquid crystal displays (LCD), touch screens, plasma displays, transparent film heaters, organic light emitting diodes (OLEDs), organic photovoltaic devices (OPVs) and solar cells (Figure 1.1). The combination of optical transparency and electrical conductivity provides the possibility to extract electrical carriers while transmitting light through the layer. Because of these properties, many scientific researches have been performed to explore different possibilities for the fabrication of TCEs exhibiting a good compromise between optical transparency and electrical conductivity. Therefore, the two most important criteria for these electrodes are low sheet resistance and high transmittance.

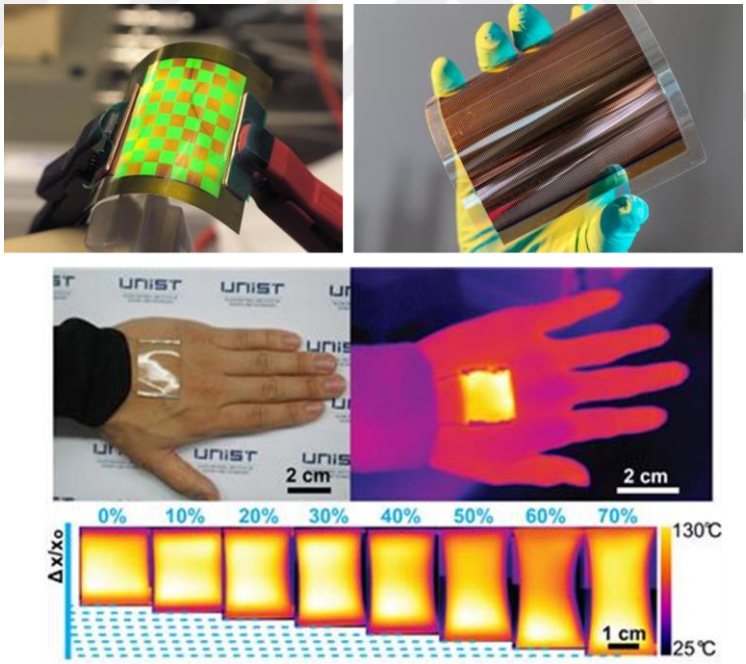

Figure 1.1 : Examples of OLED, OPV and film heater applications.

Currently indium-tin-oxide (ITO) is mainly used as TCE, because of its low sheet resistance and high optical transmission. ITO has demonstrated the optoelectronic properties of 10-20 Ω/□ with >80% optical transmittance in the visible range. However, ITO has several disadvantages including high price in indium source,

fragile nature and high production costs. The fragile nature of ITO limits its use in flexible applications, which are regarded as a new technology. Besides, post heating processes are required to increase conductivity of ITO, resulting in additional cost. Therefore, alternative solution processing materials are necessary to replace ITO for solving these drawbacks. Various solution-processable materials, such as graphene, conducting polymers (PEDOT:PSS), carbon nanotubes (CNTs), silver nanowires (AgNWs) and hybrid of these materials have been studied by many research groups (Figure 1.2).

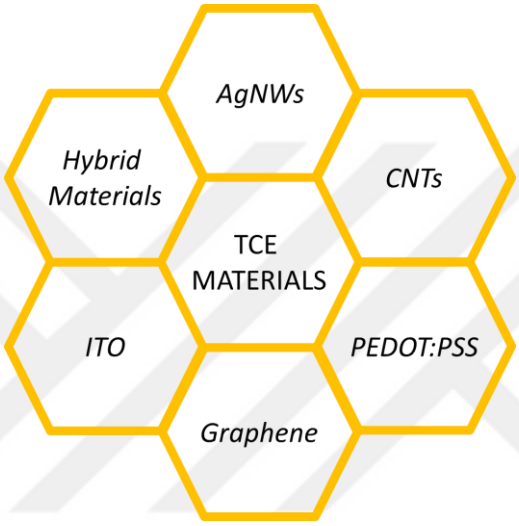

Figure 1.2 : Materials for transparent conductive electrodes.

Graphene has been widely used as an alternative material. It has great potential in many applications because of its unique properties including large surface area, high chemical resistance, high carrier mobility, high thermal and electrical conductivity, ease of surface modification, and excellent electrocatalytic activity. Moreover, a graphene oxide (GO) layer can prevent the oxidation of metalic nanowires in a hybrid film due to the gas barrier characteristic of graphene. GO laminates the metalic nanowires surface by filling empty space, resulting in a smooth surface. The oxygen-containing functional groups on GO layer such as hydroxyl and carboxylic acid lead to prevention of electron transfer, resulting in electrical insulator GO. These functional groups gain a hydrophilic property for GO and provide highly disperse solutions in aqua media. Solution processable property of GO allows chemical functionalization of the GO to use in various applications.

PEDOT:PSS is another alternative to replace ITO. It is a widely used conducting polymer. The polymer has interesting properties, such as low cost, easy processable

and good flexibility. Recently, the conductivity of PEDOT:PSS (100-1000 $S.cm^{-1}$) has continuously performed by using different approaches. However, its high sheet resistance with 10^2-10^3 Ω/□ is significantly higher than ITO (10-20 Ω/□), which in turn results in lower power conversion efficiencies (PCEs) in organic photovoltaics (OPVs). In addition, PEDOT:PSS shows poor stability in the presence of moisture, because it degrades in air atmosphere in a short time.

CNTs are considered to be a promising candidate due to their unique optical and electrical properties together with their superior mechanical flexibility and chemical stability. To date, CNTs, including single-walled and multi-walled, have been frequently used to fabricate TCEs for touch screens, OPV and OLED devices. The typical sheet resistance of CNT network is reported in the range of 10^2-10^4 Ω/□ with ~80% optical transmission at 550 nm.

Silver nanowires (Ag NWs) have emerged as a promising candidate due to their low inherent resistivity, high optical transmission and excellent flexibility. Since the diameter of the Ag NWs is usually less than 100 nm and the aspect ratio is higher than 100, percolation threshold could easily be formed. Moreover, highly mature large-scale synthesis protocol is available for the Ag NWs. In addition, the as-synthesized Ag NWs solution could be coated with any kind of solution processing techniques both on rigid and flexible substrates. The typical reported sheet resistance values are in the range of 1-100 Ω/□ with optical transmission of 80-90%, which is advantageous for OPV applications.

There are a variety of solution based coating methods to produce transparent conductive film, including drop-casting, spray coating, brush painting, spin coating and meyer-rod-coating. These solution processes are all cost competitive with conventional vacuum deposition for ITO production and produce an electrode with low sheet resistance and high transmittance. However, the difficulties in large area coating and the challenges in obtaining uniform films are the significant disadvantages of these techniques. In addition, large amounts of waste material after coating and the problems in viscosity adjustments are other major drawbacks of mentioned methods.

On the other hand, LBL is a promising method among the thin-film deposition techniques (Figure 1.3). In fact, LBL method has mainly been utilized for preparation of functional multilayers. More recently, gold and silver nanoparticle multilayers

have been fabricated via LBL deposition by different research groups for fabrication of electrode, chemical sensors, biosensors, electrochemical, electronic and optical devices. Major advantage of LBL deposition is that it allows one to control the structure of the coatings with actual nanometer scale precision, which includes both normal and lateral packing of the nanoscale building blocks. In other words, it is very easy to control film thickness and morphology, and thus easy to fabricate 3-D interconnected nanomaterial blocks. Generally, the adhesion of the multilayer film to the substrate is very good since the multilayer is formed via covalent bonding or ionic interaction. Therefore, nanomaterial multilayers via LBL deposition have been widely studied for fabrication of sensors, biosensors, functional composite films, electrochemical devices and transparent conductive electrode. In the case of fabrication of transparent conductive electrode via LBL deposition, nanomaterials with negatively and positively charged were deposited on the substrate alternatively. The main disadvantage of this approach is the presence of surfactant and polymer in the multilayer, which led to an increase in the sheet resistance, owing to their insulating property. Recently, Hammond group demonstrated the LBL deposition of multi-walled CNTs chemically functionalized with carboxylic acid and amine moieties without using any surfactant and polymers. However, this approach has never been utilized for fabrication of transparent conductive electrode.

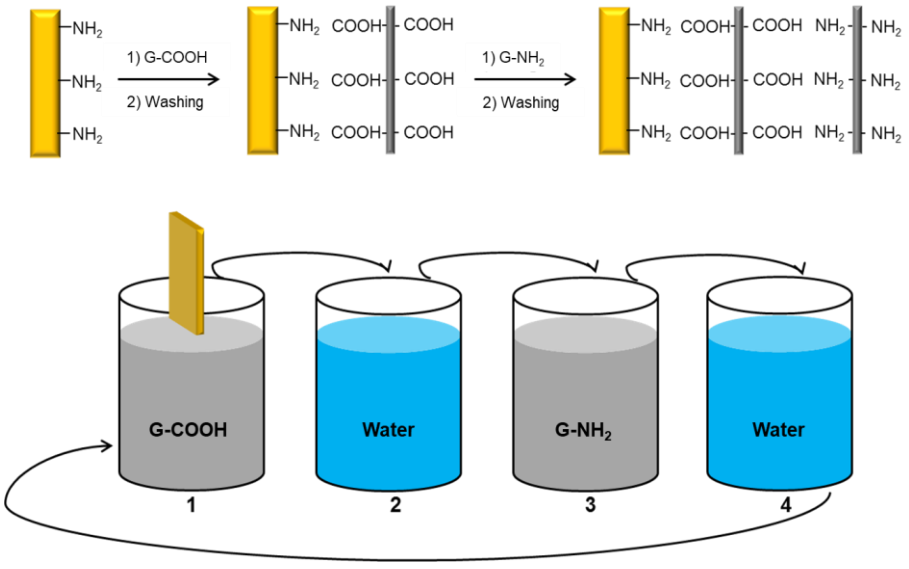

Figure 1.3 : Schematic illustration of LBL process.

1.1 Purpose of the Thesis

The objective of the thesis is to preparation of transparent conductive electrodes alternative to ITO. Various novel nanomaterials have functionalized and coated on rigid or flexible substrates by layer by layer deposition. During the thesis, microscopic (AFM, SEM, Optical Microscope), electronic (Four point probe) spectroscopic (UV, FT-IR, XRD, XPS, Zeta Potential) and thermographic (TGA, DSC) analyses are performed for the characterization of functional nanomaterials. Thesis is organized in such that each chapter has its own introduction, experimental, results and discussion sections.

Chapter 2 represents a novel approach in terms of transfer of multilayered carbon nanotubes from glass to flexible polymer substrate. This approach eliminates the use of surfactants as well as the detrimental effects of chemical and thermal treatments on the polymer substrate. Flexible transparent conducting electrodes were prepared on a polymer substrate with a multilayer transfer of oppositely charged carbon nanotubes coated on glass substrate via layer by layer deposition.

Chapter 3 shows the preparation of a highly transparent and conductive silver nanowire films. In the approach, surface modification and layer by layer assembly are unique aspects. Highly transparent and conductive electrodes demonstrated that can be used in various applications alternative to ITO.

Chapter 4 describes the fabrication of flexible transparent film heaters using functional silver nanowires. Optoelectronic, thermal, morphological and mechanical performance of the layer by layer assembled films were extensively studied.

2. PREPARATION OF TRANSPARENT CONDUCTING ELECTRODE ON POLYSULFONE FILM VIA MULTILAYER TRANSFER OF LAYER-BY-LAYER ASSEMBLED CARBON NANOTUBES [1]

Owing to their lightness and bendability, transparent conductive electrodes (TCEs) coated on a flexible substrate has attracted considerable attention for next-generation optoelectronic devices, such as displays, touch screen panels, organic photovoltaics (OPV) and organic light emitting diodes (OLED) [1-3]. Indium tin oxide (ITO) has been the most widely utilized TCE material due to its high optical transmittance and low sheet resistance. However, ITO's inherent brittleness makes it unfavorable for possible future flexible optoelectronic applications [4,5].

Therefore, significant research effort has been devoted to identifying alternativematerials to replace ITO, including carbon nanotubes (CNTs), graphene, conducting polymers and silver nanowires [6-9]. Among these materials, CNTs are considered to be a potential candidate due to their unique optical and electrical properties together with their superior mechanical flexibility and chemical stability [10]. To date, CNTs, including single-walled and multi-walled, have been frequently used to fabricate TCEs for touch screens [11], OPV [12-14] and OLED devices [15].

Typically, air-spray coating [16-18], dip coating [19,20], electrophoretic coating [21,22], ultrasonic spraying [23], rod coating [24,25], transfer printing [26] and brush painting [14] have been utilized for preparation of CNT-based TCEs. Prior to coating in these approaches, the CNTs were dispersed in water using surfactants followed by treatmentwith an ultrasonic probe to obtain a stable solution. However, surfactants are known to be insulators, which lead to an additional, labor intensive removal step after coating. In addition, the films possess irregular morphologies and significant roughness, which may result in shortcircuits and poor reproducibility during device fabrication. In addition, chemical and/or thermal treatment is frequently necessary to increase the conductivity of the CNT films, which may be detrimental to the flexible polymer substrate.

[1] This chapter is based on the paper " Oytun F., Dizman C., Karatepe N., Alpturk O., and Basarir F., Preparation of transparent conducting electrode on polysulfone film via multilayer transfer of layer-by-layer assembled carbon nanotubes. Thin Solid Films, 2017, 625, 168-176."

Multilayer transfer printing (MTP) is an exciting technique where a multilayer polyelectrolyte film is assembled on a polydimethylsiloxane (PDMS) stamp and transferred to another substrate via electrostatic interactions [27]. The Hammond group introduced the MTP technique to prepare thickness controlled polyelectrolyte multilayer patterns. This approach has subsequently been extended to obtain electrically conductive [28] and electroactive films [29].

In this study, flexible TCEs are prepared using a novel approach, called the multilayer transfer, that is very similar to the MTP is presented. This technique depends on the layer-by-layer (LBL) assembly of oppositely charged CNTs on a glass substrate, followed by transferring the CNT film to a transparent, flexible polymer substrate by means of various chemical interactions. This approach eliminates the use of surfactants as well as the detrimental effects of chemical and thermal treatments on the polymer substrate. First, the CNTs were functionalized to obtain negatively and positively charged samples. Second, the multilayered CNT electrodes were fabricated via LBL assembly onto glass substrates and subjected to chemical and thermal processes to improve the electrical properties. Next, the CNT multilayer films were transferred to the PSU substrate to obtain a flexible TCE. Finally, the transparent electrode was demonstrated to be a resistive touch sensor.

2.1 Experimental

2.1.1 Materials

Pristine single-walled carbon nanotubes (SWCNTs) were provided by OCSiAl (www.ocsial.com). Iron (III) nitrate nonahydrate ($Fe(NO_3)_3 \cdot 9H_2O$), magnesium oxide (MgO), sodium hydroxide (NaOH), dichloromethane (CH_2Cl_2, ≥99.8%), hydrochloric acid (HCl, 37%), perchloric acid ($HClO_4$, 60%), sulfuric acid (H_2SO_4, 95–98%), nitric acid (HNO_3, 60%) and ethylenediamine (EDA, ≥99%) were purchased from Merck. N,N′-dicyclohexylcarbodiimide (DCC, 99%) and 1-[Bis(dimethylamino)methylene]-1H-1,2,3-triazolo[4,5-b]pyridinium1- oxide hexafluorophosphate (HATU, 99%) was obtained from Alfa Aesar while commercial polysulfone (PSU, Mw: 29,000 g/mol) was provided from Solvay Advanced Polymers. Microscope slides (ISOLAB) with dimensions of 76 × 26 × 1 mm were used as the glass substrate. All aqueous solutions were prepared with deionized water (DI, 18.2MΩ) with a Millipore-Q system.

2.1.2 Synthesis and functionalization of CNTs

MWCNTs were synthesized according to our reported procedure by chemical vapor deposition (CVD) method with acetylene (C_2H_2) as the carbon source [30]. Carboxylic acid functionalized MWCNTs (MWCNT-COOH) were prepared based on a reported protocol [31]. Briefly, 1 g of MWCNTs were treated with 100 ml of concentrated H_2SO_4/HNO_3 (3/1, v/v) at 70 °C for 6 h. The productwas subsequently diluted with 100 ml of DI water followed by filtering through a 0.45 μm polytetrafluoroethylene (PTFE) membrane and drying in a vacuum-oven at 80 °C for 12 h. Amine-functionalized MWCNTs (MWCNT-NH_2) were prepared based on a procedure in the literature [32]. The dried MWCNT-COOH was sonicated and suspended in 20 ml of EDA under stirring and heating. After 5 min, 0.625 g of DCC was added into the suspension and mixed at 100 °C for 96 h. The product was filtered through a PTFE membrane filter, washed with ethanol and dried in a vacuum-oven at 80 °C for 12 h. Carboxylic acid (SWCNTs-COOH) and amine functionalized SWCNTs (SWCNTs-NH_2) were prepared according to the procedure performed by Brinson et al. [33]. To obtain carboxylic acid functionalized SWCNTs (SWCNTs-COOH), 30 mg of purified SWCNTs were added to 30 ml of concentrated H_2SO_4/HNO_3 (3/1, v/v) and sonicated for 3 h at 40 °C in an ultrasonic bath. The resulting mixture was diluted with 100 ml deionized water and then filtered through a 0.45 μm PTFE membrane. The product was dried in vacuum-oven at 80 °C for 12 h. For the amine-functionalized SWCNTs (SWCNTs-NH_2), 10 mg of dried SWCNTs-COOH were dispersed in 5 ml of EDA and 0.5 mg of HATU was added to the mixture. The resulting mixture was sonicated for 4 h in an ultrasonic bath. The product was diluted with 100 ml methanol and filtered through a 0.45-μm PTFE membrane. The final product was then dried in a vacuum-oven at 80 °C for 12 h. Finally, all functionalized CNTs were sonicated in DI water to form a stable dispersion with a concentration of 0.1 mg/ml. The pH was adjusted to 2.5 for MWCNTs-NH_2 and SWCNTs-NH_2 solutions and 3.5 for MWCNTs-COOH and SWCNTs-COOH using 0.1 M HCl or 0.1 M NaOH.

2.1.3 Preparation of CNT multilayer films

Prior to the coating, the glass substrates were ultrasonically cleaned in acetone and ethanol for 10 min and dried with pure N_2. Next, the substrates were treated with O_2

plasma for improved wettability (30 W, 30 s) [34]. The CNT multilayer electrode (MWCNT and SWCNT) on glass substrates was obtained via LBL deposition of oppositely charged CNT-NH_2 and CNT-COOH in an automatic slide stainer (Sakura DRS-2000). Briefly, the substrates were first immersed into the CNT-NH_2 solution for 15 min, followed by washing with DI water. Next, the substrates were dipped into the CNT-COOH solution for 15 min and were then washed with DI water. This process was repeated up to 20 times. Schematic representation of the LBL process is shown in Figure 2.1a.

2.1.4 Post treatment of CNT multilayer

To reduce the sheet resistance, the CNT multilayer electrodes were subjected to chemical and thermal post treatments. For the chemical treatment, the as-prepared films were immersed into various acidic solutions, including nitric acid, sulfuric acid, hydrochloric acid and perchloric acid, and the immersion time was varied from 30 min to 5 days. The acid treated films were then vigorously rinsed with DI water to remove residues and dried under N_2 flow. For thermal treatments, the films were annealed under air, hydrogen or vacuum. The thermal treatment temperature was varied from 200 °C to 400 °C whereas the treatment time was changed from 30 to 300 min. All post-treatments were performed with 12-bilayer CNT films.

2.1.5 Multilayer transfer

The PSU solution was prepared by first dissolving the PSU in dichloromethane (b.p. 40 °C) with a concentration of 50 mg/ml. 100 µl of the PSU solution was dispersed on the CNT multilayer coated glass substrate and allowed to dry at RT for 5 min. Then, the PSU film was easily peeled off from the glass substrate, which resulted in full transfer of the CNT multilayer to the PSU film. A schematic representation of the multilayer transfer process is demonstrated in Figure 2.1b.

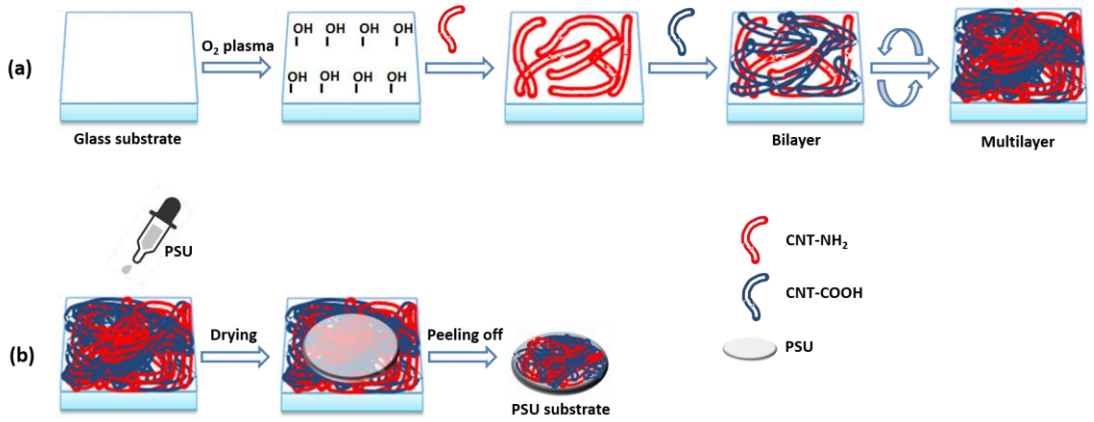

Figure 2.1 : Schematic illustration of (a) LBL and (b) multilayer transfer processes.

2.1.6 Characterization

Zeta potential (Nano ZS, Malvern Instruments, UK) measurements was carried out to determine the surface charge of CNTs. The optical transmittance of the films was measured with a UV–Vis spectrophotometer (Lambda 750, Perkin-Elmer, USA) and the sheet resistance of the films was measured using the four-point probe method (Jandel RM3000). The morphology of the CNT films was studied by field emission scanning electron microscopy (FE-SEM, JEOL 63335F JSM) and atomic force microscopy (AFM, Bruker Dimension Icon). Touch sensor properties of the flexible TCE film was evaluated by placing the film on a printed circuit board with an electrode distance of 5 mm. Current passing through the film was measured with a digital multimeter, which was connected to an LED.

2.2 Results and Discussion

Figure 2.2 shows the zeta potentials of functionalized CNTs as a function of pH with a concentration of 0.1 mg/ml. The MWCNTs-COOH and SWCNTs-COOH possess negative surface charges over the pH range from 2 to 8. In addition, the surface charge of the MWCNT-COOH and SWCNTs-COOH decreased with the decreasing pH, which could be attributed to the protonation of the carboxyl groups in agreement with Hammond's work [31]. On the other hand, the MWCNTs-NH_2 and SWCNTs-NH_2 have positive surface charges in the same pH range. The surface charges of the MWCNT-NH_2 and SWCNTs-NH_2 increased with the decreasing pH, which could be explained by the changes in the ionization degree of the amine groups [31]. Generally, particles with a zeta potential in the range of −30 mV to +30 mV were

reported to be stable due to strong electrostatic repulsion [35]. Therefore, the pH of the CNTs-COOH and CNTs-NH_2 solutions were adjusted to 3.5 and 2.5, respectively.

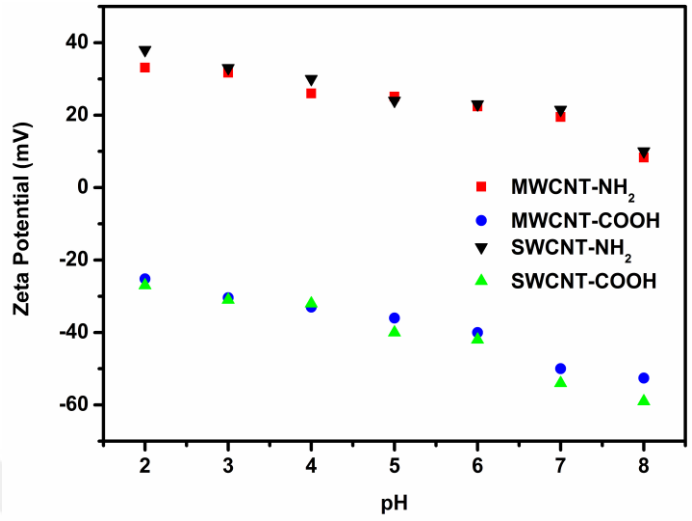

Figure 2.2 : Zeta potential of all functionalized CNT solutions.

Optical images of the LBL assembled MWCNT and SWCNT films on glass substrates are shown in Figure 2.3. As the number of layers was increased, the film color became darker. The increase in thickness is same for each deposition step demonstrating the equal amount CNTs deposited.

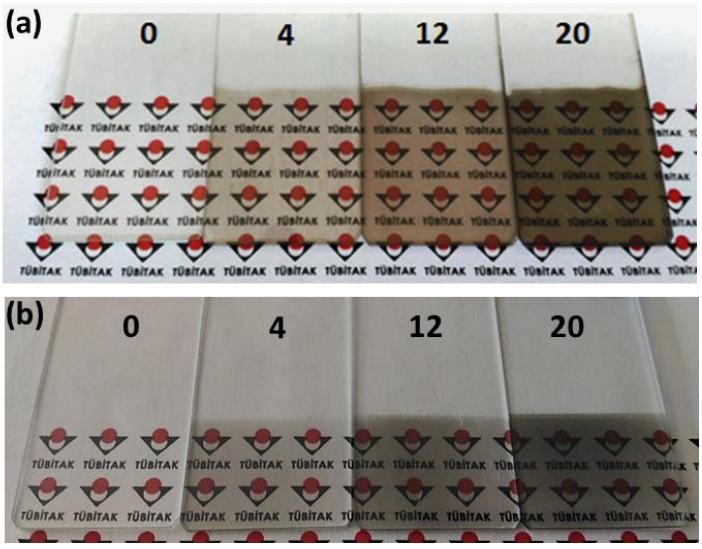

Figure 2.3 : Optical images of (a) as-prepared MWCNT films (b) as-prepared SWCNT films with different bilayer numbers on the glass substrates.

In association with the optical images, the transmittance of the LBL assembled MWCNT and SWCNT at 550 nm was found to decrease linearly with the increasing

number of bilayers (Figure 2.4), demonstrating the successful sequential deposition of oppositely charged CNTs. In addition, the successful LBL deposition of functionalized CNTs was also demonstrated with the decrease in sheet resistance as the number of layers increased (Figure 2.4), which in turn led to more continuous pathways for electron transport. For instance, the 12-bilayer MWCNT film provided transparency and sheet resistance of 68% and 43 kΩ/□, while the 12-bilayer film of SWCNT film provided a transparency and sheet resistance of 81% and 400 Ω/□, respectively. The measured sheet resistances are well above the requirements of modern optoelectronic devices. Therefore, as-prepared films were subjected to various post treatment processes to improve the electrical conductivity without deteriorating the optical transmission.

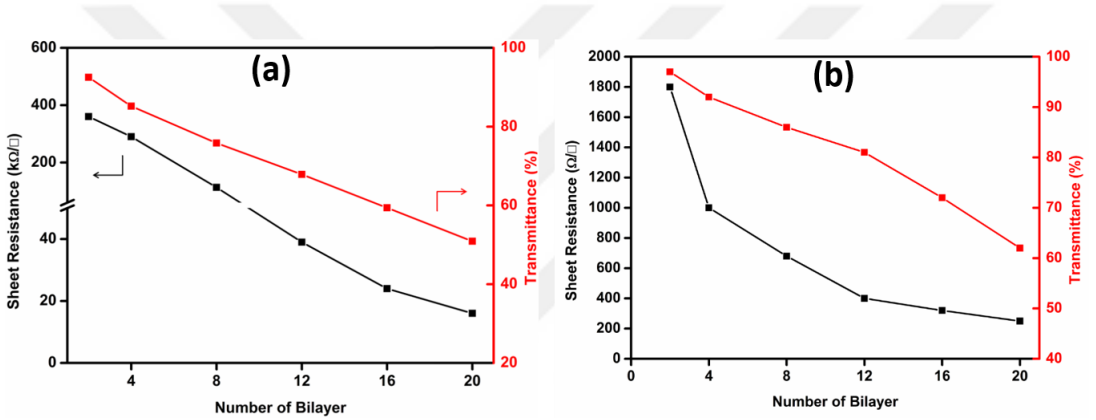

Figure 2.4 : Sheet resistance and transmittance of as-prepared films as a function of the number of bilayers on a glass substrate for (a) MWCNT films and (b) SWCNT films.

First, the effect of immersion time in various acids on the sheet resistance of the 12-bilayer MWCNT film was investigated, as illustrated in Figure 2.5a. It is worthy to note that the sulfuric acid has the strongest effect on the sheet resistance. This effect is likely attributable to the high p-doping effect of sulfuric acid in comparison with other acids [36]. HNO_3 is another effective acid to reduce the sheet resistance. Graupner et al. showed by XPS analysis that H_2SO_4 and HNO_3 caused p-doping in CNT films. In addition, it was claimed that the most stable doping and lowest sheet resistance were obtained using H_2SO_4 [37]. Typically, the sheet resistance decreased remarkably with a dipping time up to 1 h and leveled off after 2 h. In contrast, the longer treatment time caused a slight increase in the sheet resistance. This might be explained by the defects formed on the nanotube walls [38]. The lowest sheet resistance (13 kΩ/□) was obtained with the sample treated in H_2SO_4 for 2 h.

Meanwhile, the influence of the thermal treatment on the sheet resistance of the MWCNT films was also explored with respect to the treatment time, temperature and atmosphere (Figure 2.5b). It is noted that all the thermal treatment methods resulted in reduced sheet resistances. There is a significant decrease in the sheet resistance by increasing the treatment temperature from 200 °C to 400 °C in air. The increased temperature from 200 to 400 °C for a 30-min treatment resulted in an improved sheet resistance. However, it is interesting to note that when treatment at 400 °C was performed >30 min, no electrical conductivity could bemeasured, indicating the decomposition of the CNT network. This was affirmed by TGA and FE-SEM analysis (not shown here). In addition, treatment at 150 °C under vacuum provided sheet resistance values comparable to treatment at 200 °C in air. However, thermal treatment at 300 °C under H_2 atmosphere provided the lowest sheet resistance (8.4 kΩ/□), which might be explained by the burning off of oxygen-containing functional groups on the MWCNTs. The same post treatment processes were also used for the 12 bilayer SWCNT film. Similar trends were seen in the post treatment processes of the SWCNT film, as shown in Figure 2.5c and d. When the film was treated in H_2SO_4 for 2 h, the sheet resistance decreased from 400 Ω/□ to 107 Ω/□. In the case of thermal treatment performed at 300 °C under H_2 atmosphere for 2 h, the sheet resistance was measured as 130 Ω/□.

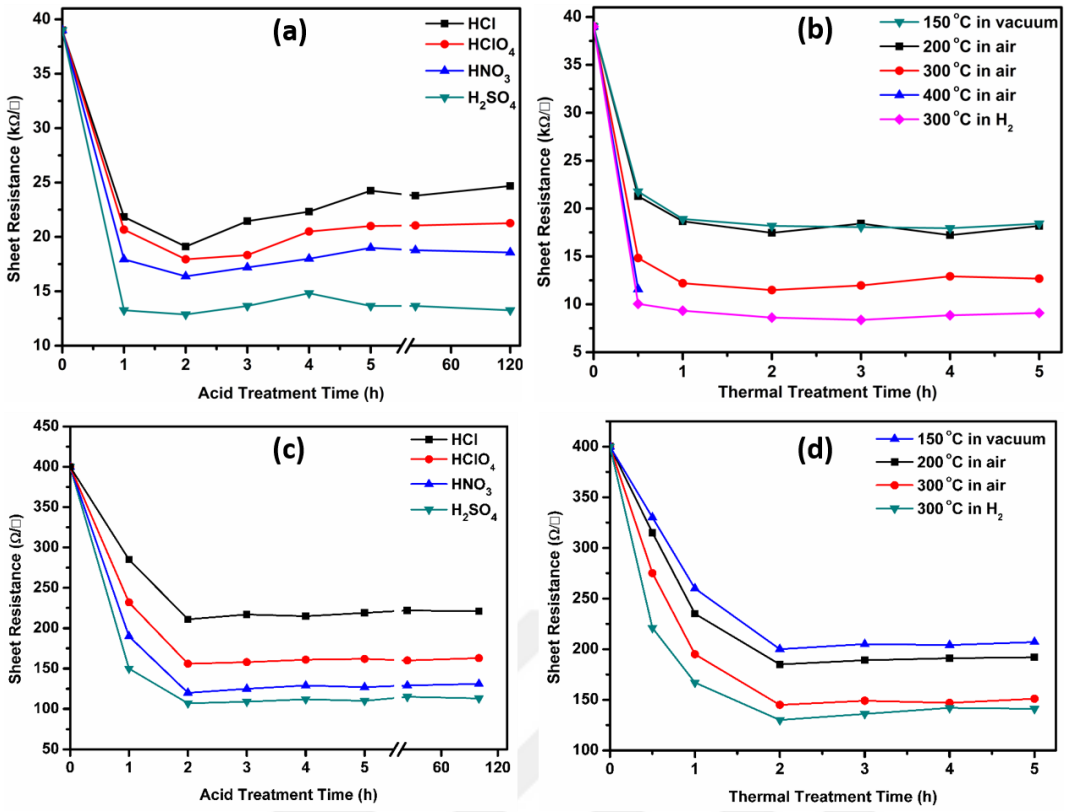

Figure 2.5 : Change in the sheet resistance for the 12 bilayer MWCNT film as a function of (a) acid treatment time and (b) thermal treatment time. The change in the sheet resistance for the 12 bilayer SWCNT film as a function of (c) acid treatment time and (d) thermal treatment time.

Morphology of the as-prepared and acid-treated (H_2SO_4 for 2 h) MWCNT films with 12-bilayers were examined with an FE-SEM (Figure 2.6a,b). Several impurities (shown by arrows) embedded within the CNT network were observed in the as-prepared film (Figure 2.6a). These impurities are believed to hinder charge transport, which led to a higher sheet resistance. After the acid treatment, impurities were removed from the MWCNT network, and the conductivity of the film was increased. Moreover, the SEM images of as-prepared and acid treated (H_2SO_4 for 2 h) SWCNT films with 12-bilayers are shown in Figure 2.6c and d. The images show that impurities on the surface were also removed from the SWCNT network after the acid treatment, demonstrating the similar morphology with that of the MWCNT film. Similarly, thermal treatment also eliminated the impurities in the film, which explains the decrease in the sheet resistance for both MWCNT and SWCNT films (not shown here).

The surface roughness of these films was investigated by AFM. While the surface roughness of the as-prepared film was ~31 nm, the surface roughness of the acid-

treated and thermal-treated films was approximately 25 and 22 nm, respectively. The samples with the smoother surface resulted in lower sheet resistance, which agrees with previous results [39].

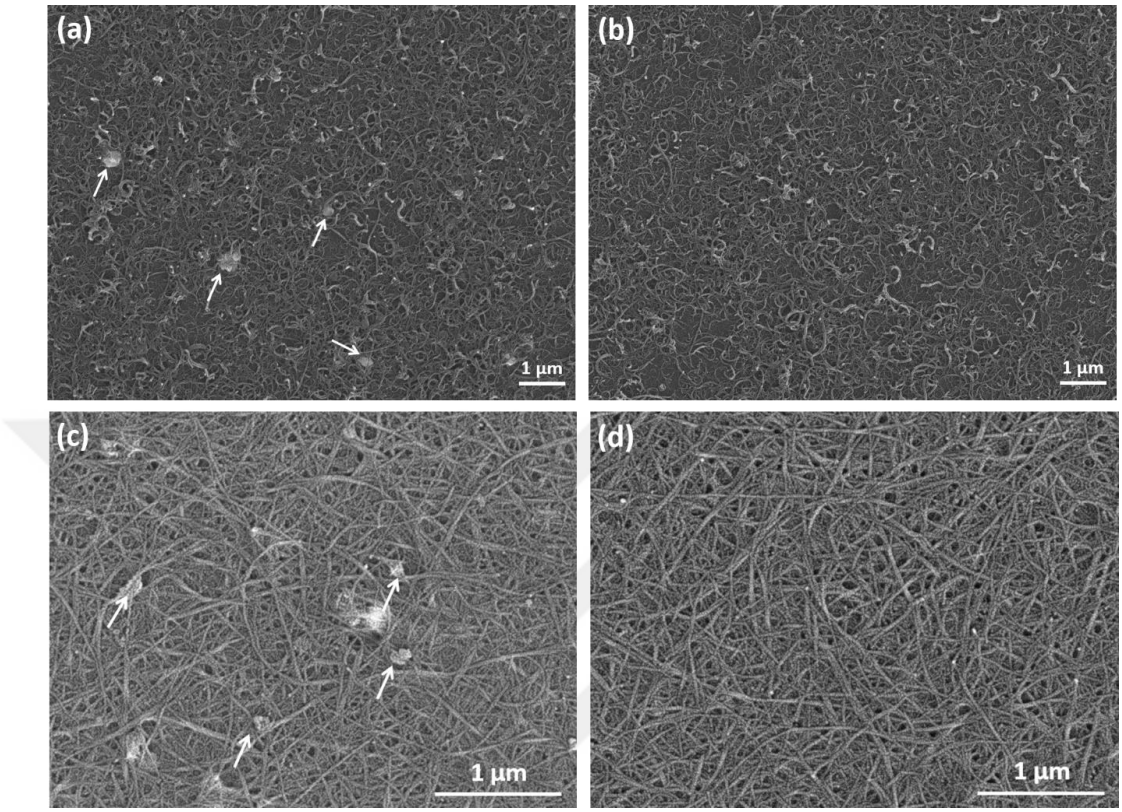

Figure 2.6 : SEM images of the 12-bilayer MWCNT film on a glass substrate (a) as-prepared and (b) acid-treated. SEM images of the 12-bilayer SWCNT film on a glass substrate (c) as-prepared and (d) acid-treated.

The PSU solution was dropped on a multilayer CNT film coated on a glass substrate and waited for a certain time when the solvent completely evaporated. The PSU film was peeled off from the substrate and is shown in Figure 2.7a and b. The entire CNT film was transferred from the glass to the PSU substrate leaving no residue on the glass substrate. To successfully transfer the multilayer film from the glass to the PSU substrate, the interaction between the glass and CNT-NH_2 (base layer of CNT film) should be weaker than the interaction between PSU and the top layer of the CNT (CNT-COOH) film. The successful transfer can be associated with hydrogen bonding between the sulfonic groups of the PSU and the carboxylic group of the CNT-COOH as well as π-π interactions between aromatic rings of the PSU and CNTs [40,41].

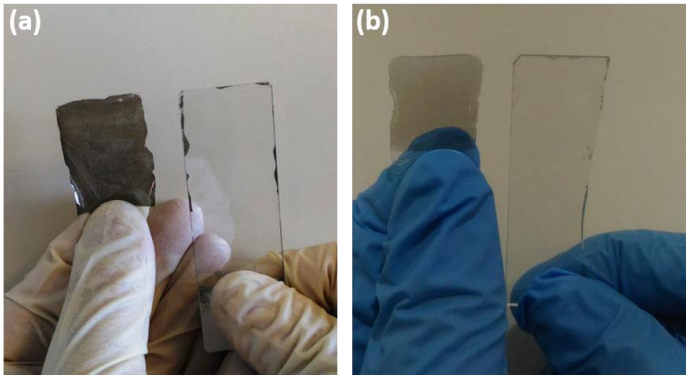

Figure 2.7 : Optical image of the (a)MWCNT film and the (b) SWCNT film transferred to the PSU substrate.

The CNT multilayer films on the PSU substrate demonstrated excellent flexibility without losing conductivity after bending 100 times, as shown in Figure 2.8a and b. The change in sheet resistance is represented by $R_{s(n)}/R_{s(0)}$ in Figure 2.8c, where $R_{s(n)}$ is the sheet resistance after n bending cycles. The sheet resistances of the flexible CNT films remained nearly unchanged after 100 bending cycles.

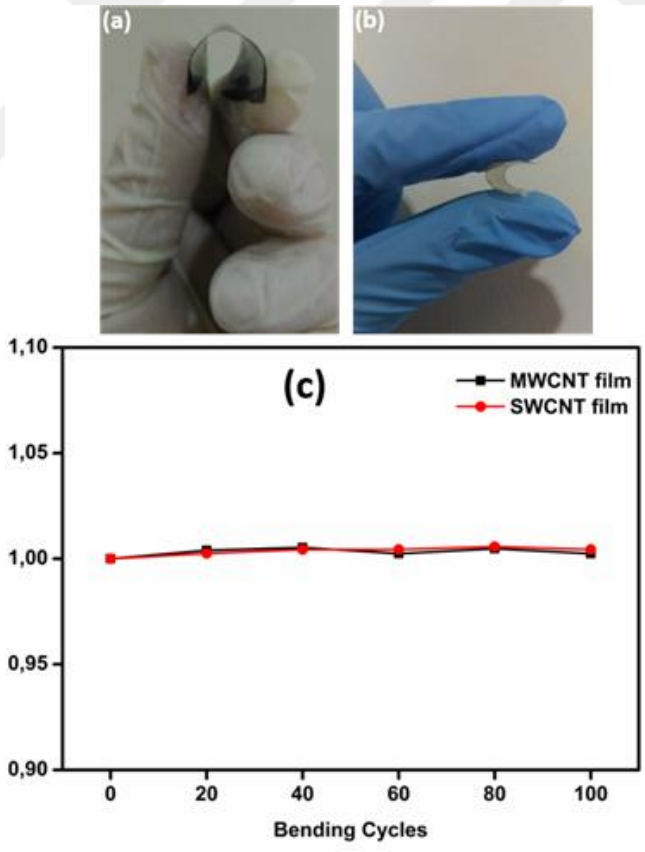

Figure 2.8 : Flexibility of the (a) MWCNT film and the (b) SWCNT film transferred to the PSU substrate. (c) The change in sheet resistance of CNT films after 100 bending cycles.

The electrical and optical properties of the transferred multilayer films are presented in Figure 2.9. After the multilayer transfer process there were no observed significant changes in the sheet resistance of all CNT multilayer film. Moreover, the sheet resistance of the films decreased with the increase in the bilayer number, which is consistent with the as-prepared films [42]. For the 12-bilayer film, the sheet resistance of the thermally treated MWCNT film decreased from 43 kΩ/□ to 8.4 kΩ/□, while the sheet resistance of the acid-treated MWCNT film decreased from 43 kΩ/□ to 13 kΩ/□. Conversely, the optical transmittance of the thermally treated MWCNT films on the PSU is shown in Figure 2.9b. As the number of layers is increased, the transmittance was observed to decrease. The obtained sheet resistance values are similar with previous works as reported by Lee et al. [31]. Figure 2.9c showed that the sheet resistance of the acid-treated SWCNT film decreased from 400 Ω/□ to 107 Ω/□ while the sheet resistance of the thermally treated SWCNT film decreased from 400 Ω/□ to 130 Ω/□. Similar trends with that of the MWCNT films on the PSU were observed in the optical transmittance of the acid-treated SWCNT films on the PSU, as shown in Figure 2.9d.

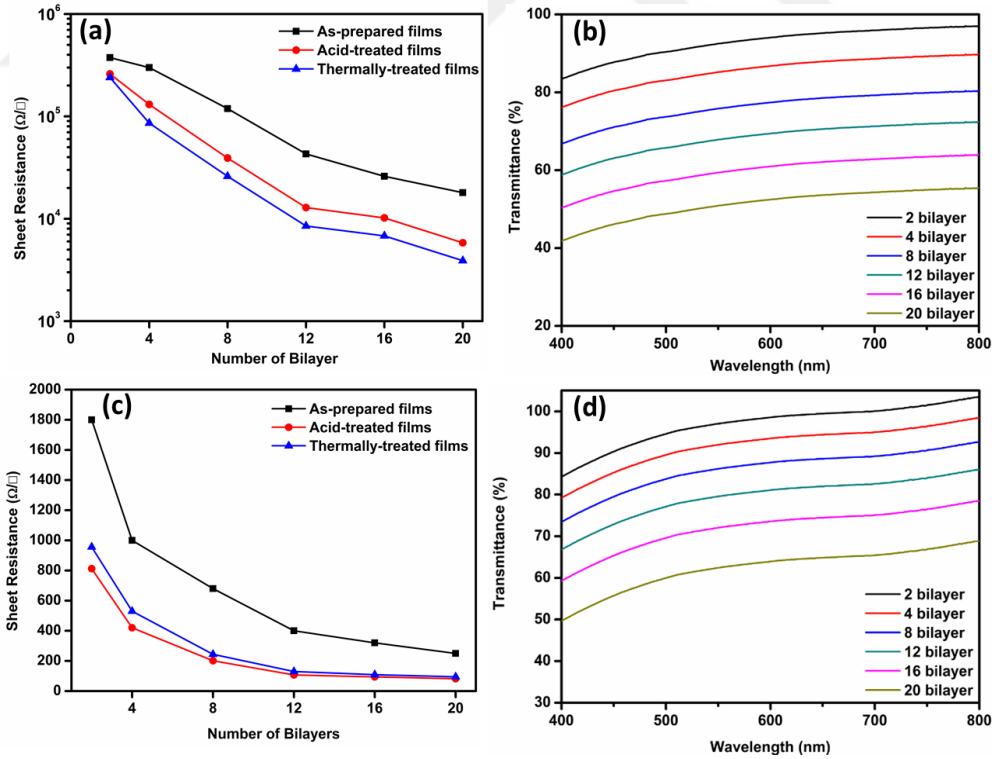

Figure 2.9 : Sheet resistances for the MWCNT films on PSU, (b) optical transmittance of the MWCNT films on PSU, (c) sheet resistance for the SWCNT films on PSU, and (d) optical transmittance of the SWCNT films on PSU.

AFM was used to characterize the surface topographic features of the MWCNT films. Table 2.1 shows the surface roughness values of the as-prepared, acid-treated and thermally treated films on PSU. The surface roughness of the films increased with the number of layers, as shown in Table 2.1. The as-prepared films presented the highest surface roughness compared to the films subjected to the posttreatment. It can be deduced that the post-treatment increased the density of the nanotubes, which led to the improved sheet resistance.

Table 2.1: Surface roughness of the MWCNT films on PSU with different numbers of bilayers.

Number of bilayers	R_q^a (nm)	R_q^b (nm)	R_q^c (nm)
4	23	18	16
12	33	27	24
20	36	29	27

a, b and c are defined as as-prepared film, acid-treated film and thermally treated film.

The performance of the transparent conducting films can be evaluated by the figure of merit (FOM) (ϕ) that depends on the sheet resistance and optical transmittance of the films. The figure of merit values were calculated using the equation defined by Haacke [43]:

$$\Phi_{TC} = T^{10}/R_s$$

where T is the optical transmittance at 550 nm and R_s is the sheet resistance. The FOM values are compared in Tables 2.2 and 2.3. The higher FOM values represent an improved performance for the transparent conducting film. While the highest figure of merit was found to be $2.52 \times 10^{-6}\ \Omega^{-1}$ for the MWCNT films with 12-bilayers, the figure of merit was found to be $1.14 \times 10^{-3}\ \Omega^{-1}$ for the SWCNT films with 12- bilayers.

Table 2.2 : FOM values for the thermally treated MWCNT films on PSU.

Number of bilayers	T (%)	R_s (kΩ/□)	ϕ_{TC} (Ω^{-1})
2	92	240	1.81×10^{-6}
4	85	86	2.29×10^{-6}
8	76	26	2.47×10^{-6}
12	68	8.4	2.52×10^{-6}
16	59	6.8	0.75×10^{-6}
20	51	3.9	0.30×10^{-6}

Table 2.3 : FOM values for the acid-treated SWCNT films on PSU.

Number of bilayers	T (%)	R_s (Ω/□)	Φ_{TC} (Ω^{-1})
2	97	812	0.91×10^{-3}
4	92	420	1.03×10^{-3}
8	86	201	1.10×10^{-3}
12	81	107	1.14×10^{-3}
16	72	94	0.40×10^{-3}
20	63	82	0.12×10^{-3}

Finally, the transparent conductive film was applied in a resistive touch sensor. When the film was attached on a printed circuit board, there was no current passing through as shown in Figure 2.10a. However, when a force is applied on the film by pressing with a finger, a current and LED lightning was observed (Figure 2.10b). Long term stability of flexible CNT films was investigated in Figure 2.10c. Even after 300 touch cycles, the sheet resistance of the flexible CNT films remained nearly unchanged, which strictly demonstrates that the CNT multilayer perfectly adheres onto the PSU.

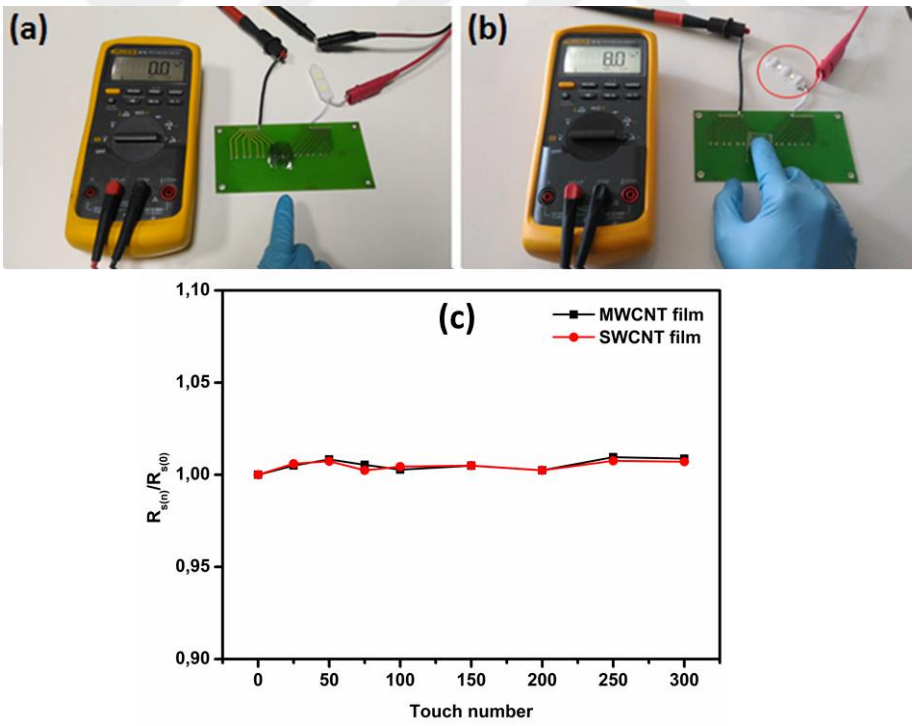

Figure 2.10 : Photograph showing the resistive touch sensor system (a) untouched state, (b) touched state with a finger and (c) stability of CNT films over 300 touch cycles.

2.3 Conclusion

Preparation of a flexible TCE based on MWCNTs and SWCNTs was successfully achieved in this work. Carboxylic acid and amine moieties were introduced on MWCNTs and SWCNTs, leading to successful LBL assembly on a glass substrate via ionic interactions. Multilayer transfer of the MWCNT and SWCNT electrodes to a PSU substrate was achieved without leaving a residue on the glass. Multilayer transfer eliminated the need of surfactants as well as the detrimental effects of chemical and thermal treatments on the polymer substrate. The highest FOM was found to be $2.52 \times 10^{-6}\ \Omega^{-1}$ at a 68% optical transmission and $1.14 \times 10^{-3}\ \Omega^{-1}$ at an 81% optical transmission for the 12-bilayer MWCNT and SWCNT, respectively. Finally, the flexible transparent conductive film was successfully demonstrated in resistive touch sensor application.

3. FABRICATION OF SOLUTION-PROCESSABLE, HIGHLY TRANSPARENT AND CONDUCTIVE ELECTRODES VIA LAYER-BY-LAYER ASSEMBLY OF FUNCTIONAL SILVER NANOWIRES [1]

Transparent conductive electrode (TCE) is a significant component of modern optoelectronic devices, including organic solar cells [44], touch screens [22] and organic light emitting diodes [2]. Indium tin oxide (ITO) is the common choice of the industry, owing to its low sheet resistance and high optical transmittance [45]. However, the brittle nature of ITO avoids its future use in next-generation flexible optoelectronic devices [4].

Therefore, in the past decade, considerable research has been conducted on alternative solution-processable materials to replace ITO. Various materials, such as silver nanowires (AgNWs) [46], copper nanowires [47], graphene [7], carbon nanotubes [48] and conducting polymers [49] have been evaluated in the literature,with AgNWs considered to be the most promising material due to their low inherent resistivity, high optical transmittance, resistance to oxidation and excellent flexibility [50,51].

For fabrication of TCEwith AgNWs, solution based coatingsmethods, such as vacuum filtration [52,53], rod coating [9], drop coating [54,55], spray coating [56], brush painting [57] and spin coating [58] techniques have been utilized hitherto. Even though, the mentioned methods provided relatively low sheet resistance and high optical transmittance values, there are several obstacles to overcome. The difficulties in large area coating and the challenges in obtaining uniform films are the significant disadvantages of vacuum filtration and drop coating techniques [59].

On the other hand, the high amount of residual solvent and the problems in viscosity adjustments are the major drawbacks of rod coating, brush painting and spray coating methods. On the other hand, layer-by-layer (LBL) deposition consisting of sequential immersion of a substrate into aqueous solutions of oppositely charged materials is a very promising approach. This method can create versatile thin filmswith highly tunable thickness, porosity, packing density and surface properties [60]. In addition,

[1] This chapter is based on the paper " Oytun F., Kara V., Alpturk O. and Basarir F., Fabrication of solution-processable, highly transparent and conductive electrodes via layer-by-layer assembly of functional silver nanowires. Thin Solid Films, 2017, 636, 40-47."

the multilayer film has excellent adhesion to the substrate since the multilayer is formed via covalent bonding or ionic interaction [61]. Thus, it has been widely utilized for fabrication of polymer [62], carbon nanotube [31], graphene [63], gold nanoparticle [64] or silver nanoparticle [65] multilayer films for various electronic and electrochemical applications. But the method has yet to be utilized for the assembly of AgNWs.

In this study, therefore, it was attempted to fabricate TCE via LBL assembly of AgNWs. The uniqueness of the presentedwork lies on the surface modification and LBL assembly of the AgNWs. First, commercial nanowires were functionalized with cysteamine hydrochloride (CA) and 3-mercaptopropionic acid (MPA) to obtain positively and negatively charged AgNWs, respectively. Then, oppositely charged AgNWs were sequentially coated on a 3-aminopropyltriethoxysilane (APTES) modified glass substrate via LBL deposition. Next, thermal annealing was carried out to enhance the electrical conductivity of the nanowire multilayer films. Finally, the AgNW multilayer film was characterized by UV–Vis spectrometer, field emission scanning electron microscope (FE-SEM), optical microscope (OM) and sheet resistance measurement by four-point probe method.

3.1 Experimental

3.1.1 Materials

Silver nanowires (AgNWs) were purchased from ACS Materials (USA) as suspension in isopropylalcohol (IPA) with a concentration of 20 mg/ml. The average length and diameter of the AgNWs were 20-30 μm and 60 nm, respectively. Cysteamine hydrochloride (CA) (BioXtra), 3-mercaptopropionic acid (MPA) (99%), 3-aminopropyltriethoxysilane (APTES) and N,N-Dimethylformamide (DMF, 99.8%) were obtained from Sigma–Aldrich. Sulfuric acid (H_2SO_4, 95-98%) and hydrogen peroxide (H_2O_2, 30%) were provided by Merck. Microscope slides (ISOLAB) were carefully cut into 76 x 13 mm^2. All aqueous solutions were prepared with the deionized water (DI, 18.2 MΩ) with a Millipore-Q system.

3.1.2 Functionalization of AgNWs

Amine-functionalized AgNWs (AgNW-NH_2) were prepared as reported earlier [66]. Briefly, CA (150 mg, 0.026 M) in DMF was added to AgNW solution (50 mg, 1

mg/ml). The reaction vessel was covered with aluminum foil and the solution was slowly stirred for 24 h at room temperature (RT). Then, the solution was centrifuged to remove the unreacted CA, followed by washing with DMF and DI water sequentially, and the final concentration was adjusted to 1 mg/ml by re-dispersing in DI water. Same procedure was implemented to obtain carboxylic acid-functionalized AgNWs (AgNW-COOH) except using MPA instead of CA. The concentration of AgNW-COOH was also adjusted to 1 mg/ml by re-dispersing in DI water. The functionalized AgNWs were kept in the dark for future use.

3.1.3 Fabrication of transparent conductive electrode

Prior to layer-by-layer (LBL) deposition, the glass substrates were cleaned by immersing into piranha solution (98% H_2SO_4 and 30% H_2O_2 with a volume ratio of 3:1) at 90 °C for 1 h, followed by rinsing with a large amount of DI water and drying with N_2 gas. *Caution: Piranha solution reacts violently with organic material and should be handled carefully*. Then, the glass substrates were dipped into 3% (v/v) APTES solution in ethanol for 2 h [67]. Next, the substrates were rinsed 3 times vigorously with ethanol and annealed in an oven at 120 °C for 1 h. Silver nanowire multilayer films were formed by LBL deposition of AgNW-NH_2 and AgNW-COOH using an automatic slide stainer (Sakura DRS-2000). First, the APTES modified glass substrates were immersed into AgNW-COOH for 15 min, followed by rinsing with DI water and blow-drying with hot air. Then, the substrates were immediately immersed into AgNWs-NH_2 for 15 min. The substrates were again rinsed with DI water and dried with hot air. The multilayer films were achieved by repeating these processes until the desired number of bilayers was reached. All coating processes were carried out at RT (~23 °C) and ~30% humidity. The multilayer films were subjected annealing to increase the electrical conductivity by varying the temperature (100–200 °C) and treatment time (15–120 min) in a tube furnace under air atmosphere.

3.1.4 Characterization

X-ray Photoelectron Spectrometer (XPS, Thermo K-Alpha) and Fourier Transform Infrared Spectrometer (FT-IR, Perkin Elmer-Spectrum Two) was utilized to characterize the chemical composition of the as-received and functionalized AgNWs. Surface charge of the AgNWs was characterized by Zetasizer (Nano ZS, Malvern

Instruments). The sheet resistance measurements of the films were performed by using 4- point probe method (Jandel RM3000) while the optical transmittance was measured with UV–Vis Spectrometer (Lambda 750, Perkin Elmer). The optical transmittance and sheet resistance measurements were carried out at RT and the average of 5 measurements were reported. Field Emission Scanning Electron Microscope (FE-SEM, JEOL JSM- 6500F) and optical microscope (Axio Scope A1, Zeiss) were used to investigate the surface topology of the multilayer films. To demonstrate the electrical conductivity of the films, a conductive path was formed on a printed circuit board. Copper wire was affixed to the end of electrodes of the printed circuit board and the contact between the AgNW multilayer film and the copper wire was obtained by silver paste. LED light was observed after applying voltage through the printed circuit board.

3.2 Results and Discussion

As-received AgNWs contain Polyvinylpyrrolidone (PVP) as capping agent, which is necessary during their synthesis. Therefore, ligand exchange process was used to introduce functional groups on the AgNWs, as demonstrated in Figure 3.1. The –SH groups of CA and MPA react with the silver atoms on the AgNW surface, which led to Ag–S covalent bonds. Thiol is known to have the highest binding affinity to noble metal surfaces (approx. 200 kJ/mol) [68].

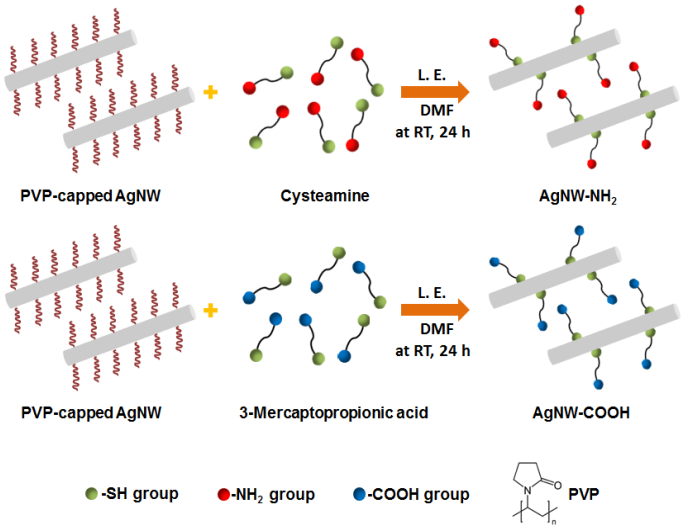

Figure 3.1 : Functionalization of AgNWs with CA and MPA.

After the ligand exchange process, XPS analysis was utilized for monitoring the surface composition of the AgNWs. The survey spectrum of AgNW-NH_2 and AgNW-COOH exhibits the expected peaks (S2p, C1s, Ag3d, N1s, O1s and Ag3p), as shown in Figure 3.2a and b. The enlarged XPS S2p core level spectrums of AgNWs-NH_2 and AgNW-COOH were shown in Figure 3.2c. The spectrums for AgNWs-NH_2 (161.9 eV) and AgNW-COOH (162.1 eV) proves the formation of S–Ag bond,which is consistent with the previous work [69]. The enlarged view of C1s spectrums were displayed in Figure 3.2d. The peaks at 284.5 and 287.6 eV could be attributed to the aliphatic carbon-carbon bond and carboxylic carbon (O–C=O), respectively [70]. In addition, there is a strong nitrogen signal at 399.2 eV in the N1s spectra of the AgNWs-NH_2, whereas no signal was observed in AgNWs-COOH (Figure 3.2d). The results confirmed the successful ligand exchange and surface modification of AgNWs with CA and MPA.

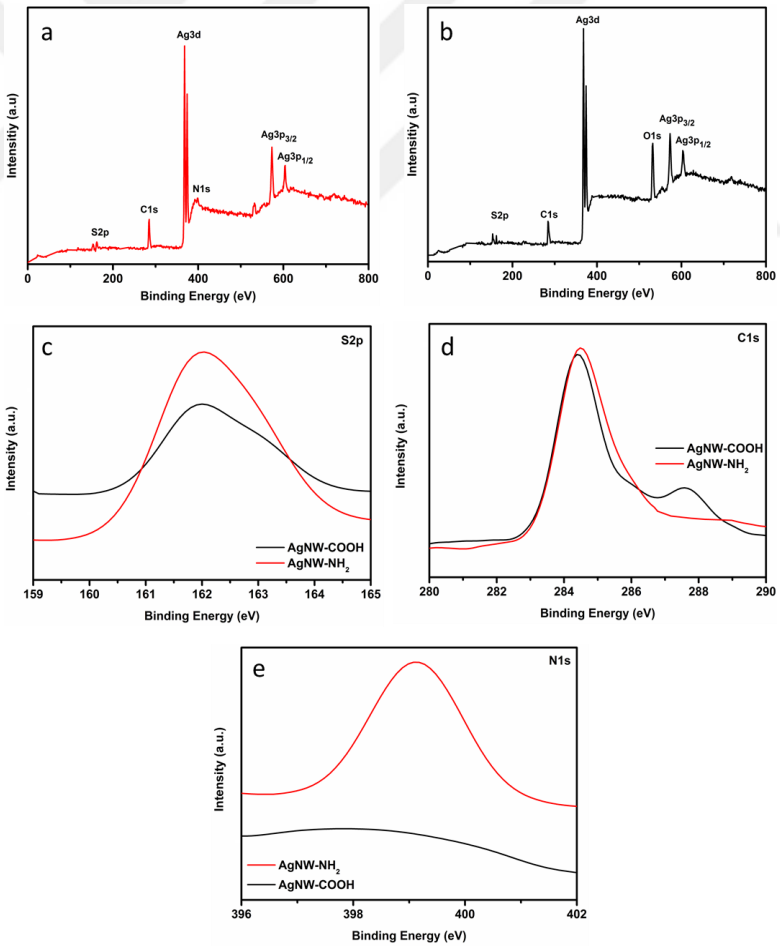

Figure 3.2 : XPS survey spectra of (a) AgNWs-NH_2 and (b) AgNWs-COOH, and (c) S2p, (d) C1s, and (e) N1s spectra of AgNWs-NH_2 and AgNWs-COOH.

On the other hand, FT-IR spectroscopy was also used to better understand the surface chemistry of the functionalized AgNWs (Figure 3.3a and b). The peaks detected at 2510 cm^{-1} in the spectrum of both CA and MPA could attributed to −SH stretching [71]. However, the loss of the −SH peaks confirms the binding of thiol groups to the nanowire surface [72]. The peak at 1446 cm^{-1} and small bands at 923 and 883 cm^{-1} in FT-IR spectra of AgNW-NH_2 could be explained by C−N stretching and NH_2 bending of amine moiety of CA, respectively (Figure 3.3a) [73,74]. Moreover, the characteristic peak at 1710 cm^{-1} of AgNW-COOH was assigned to C−O group of carboxylic acid in MPA (Figure 3.3b) [75]. These results again indicate the successful surface modification of AgNWs.

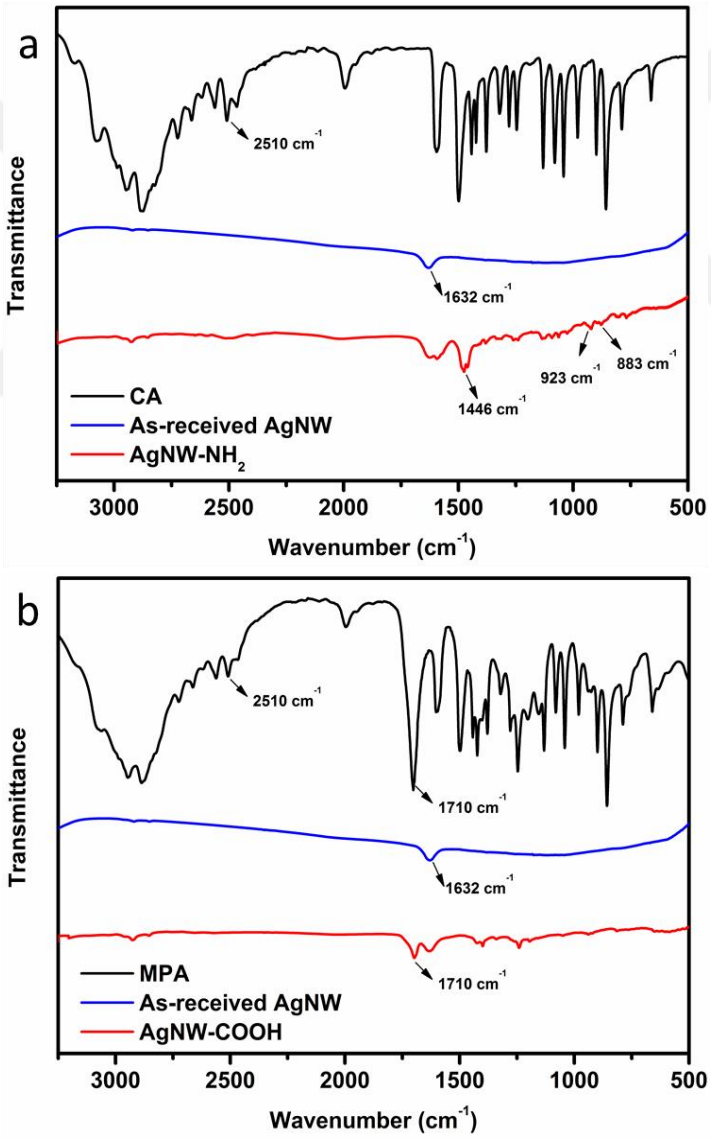

Figure 3.3 : FT-IR spectra of (a) AgNW-NH_2 and (b) AgNWs-COOH.

Surface charge of themodified AgNWs was evaluated by measuring the zeta potential of the nanowire dispersions in aqueousmedia (Figure 3.4). As expected, the AgNWs-NH_2 exhibited a positive zeta potential (+32.4 mV), while the AgNWs-COOH showed a negative value (−31.3mV). These positive and negative charges resulted from protonation of $–NH_2$ groups to $-NH_3^+$ and deprotonation of –COOH moieties to $–COO^-$, respectively [76,77]. Particles with highly negative or positive zeta potentials (+30 mV or less than −30 mV) are considered to provide sufficient mutual repulsion to ensure a stable dispersion [78], which indicates that functionalized AgNWs possessed sufficient surface charge for the stability of the dispersions.

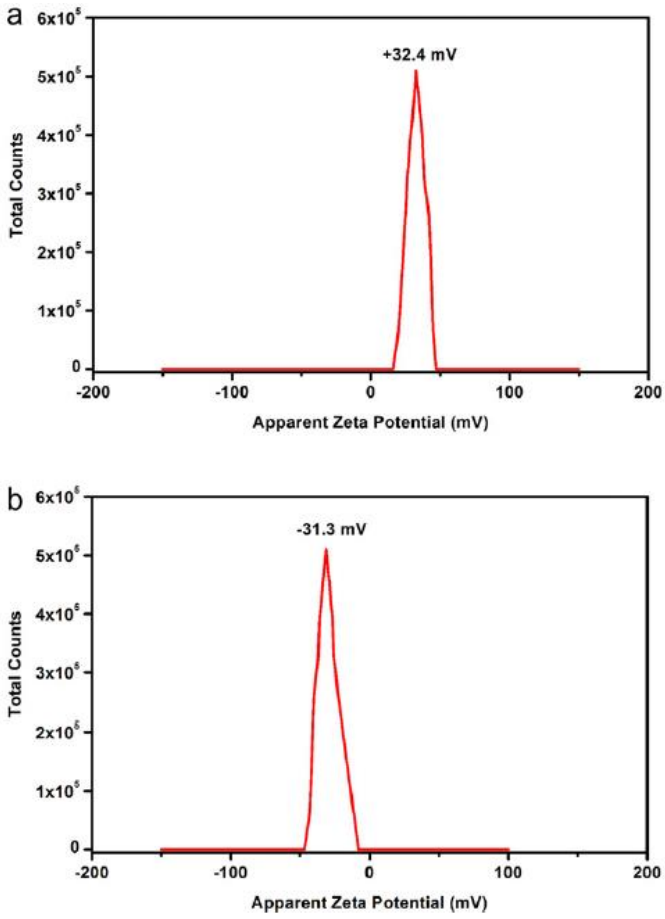

Figure 3.4 : Zeta Potential of (a) AgNW-NH_2 and (b) AgNWs-COOH dispersions.

Multilayer assembly of the silver nanowires was simply performed via electrostatic interaction between the AgNWs-NH_2 and AgNWs-COOH, as schematically demonstrated in Figure 3.5. This approach provided highly controllable nanowire thin films in terms of topology, optical transmittance and sheet resistance.

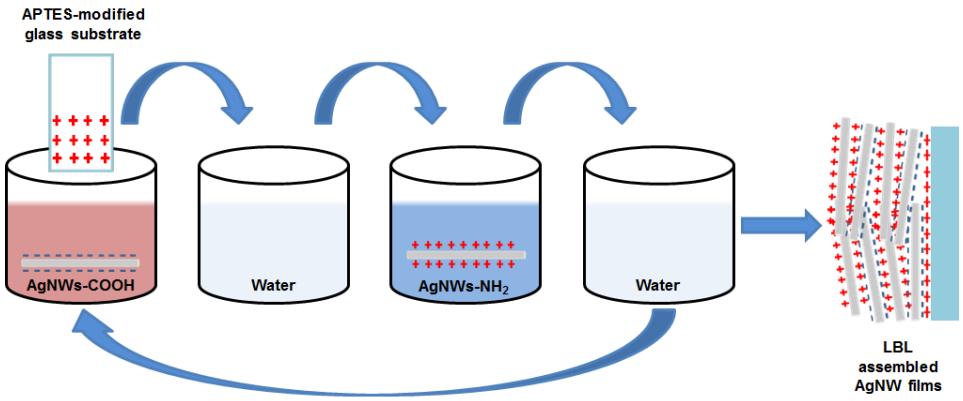

Figure 3.5 : Schematic illustration of LBL assembly of oppositely charged AgNWs.

The topology of the AgNW films was strongly influenced by the layer numbers. Optical microscope images of the said films were depicted in Figure 3.6. Increasing the layer number results in increased number of nanowires and decreased void size, which demonstrates the successful LBL deposition.

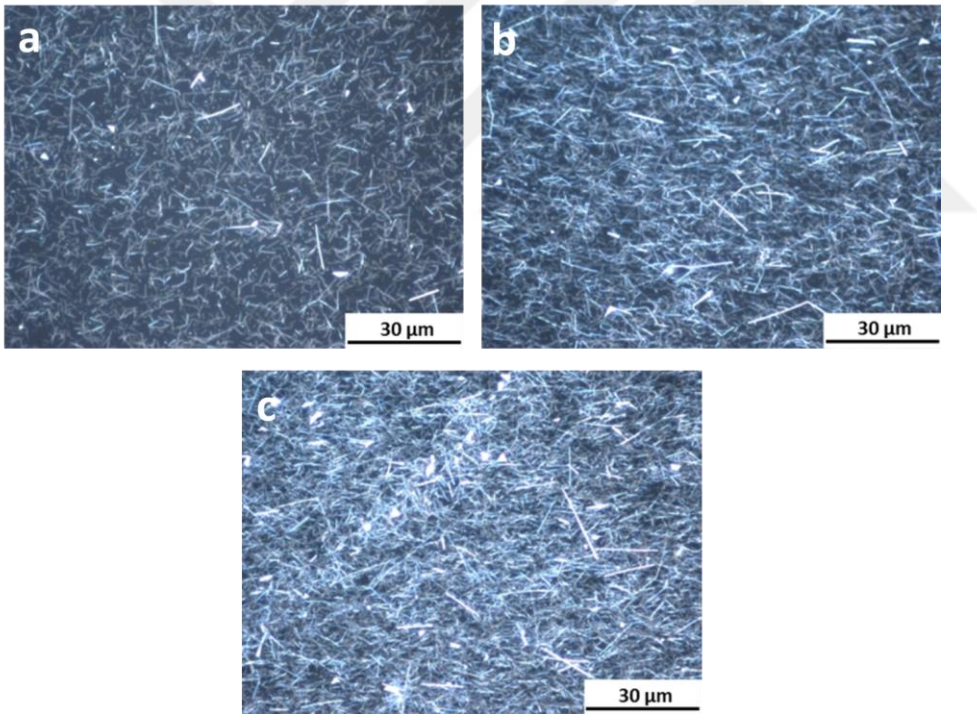

Figure 3.6 : Optical microscope images of AgNW films; (a) 2 bilayer, (b) 4 bilayer and (c) 6 bilayer.

Macro images of the LBL assembled AgNW films are shown in Figure 3.7a. Increasing the layer number provided deeper yellowish color due to the increase in the number of AgNWs, which again indicates the successful LBL deposition. It is worthy to note that the sample is still very transparent after 6 bilayer deposition. The optical transmittance analysis results are consistent with the macro and optical

images. As the number of layers increased, the optical transmittance decreased (Figure 3.7b), since the increased number of AgNW layers inhibit light transmittance, which was measured as 97.8% (@550 nm) for one bilayer and decreased gradually to 83.8%, with 6 bilayers (Figure 3.7c). There is almost a linear drop of the optical transmittance at 550 nm with indicates the deposition of same amount of material for each layer. It is worthy to note that the optical transmittance of the 6-bilayer (83.8%) sample can be compared with the commercial ITO electrodes (T= 79.5%) [79].

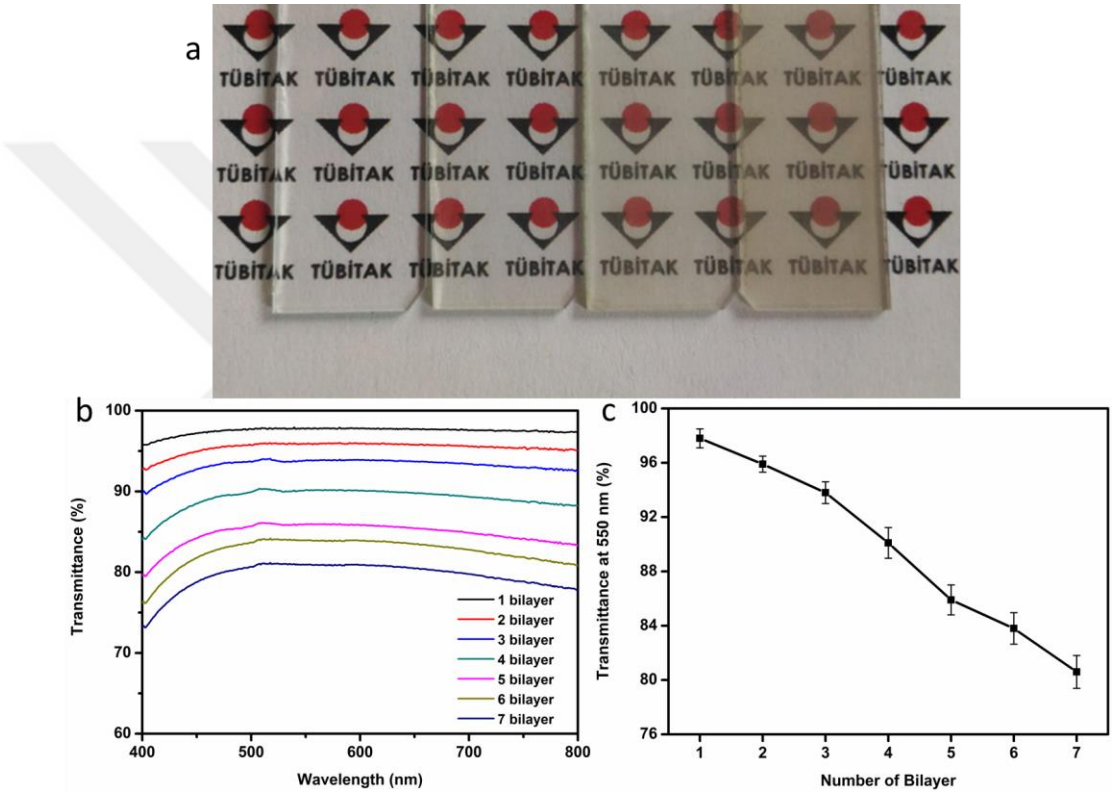

Figure 3.7 : (a) Macro images, (b) Optical transmittance and (c) Optical transmittance at 550 nm as a function of number of bilayer for LBL assembled AgNW films.

Regardless of the layer number, the as-deposited AgNW films possessed high sheet resistance (~2MΩ/□) possibly due to the organic capping molecules (CA and MPA) and thus, the films were subjected to thermal annealing. Annealing has two functions on the AgNW films; 1) removal of the insulating capping molecules from the nanowire surface and 2) surface melting of the nanowires which makes them fuse into each other [80]. Hence, annealing leads to the formation of efficient conduction pathways through the AgNW network. The annealing conditions such as temperature and time were optimized by measuring the sheet resistance of the 6 bilayer AgNW

film, as illustrated in Figure 3.8a. As the annealing temperature increased, sheet resistance decreased from ~2 MΩ/□ (as-deposited) to 65 Ω/□ (100 °C) and 32 Ω/□ (125 °C), and then increased to 61 Ω/□ (150 °C) and 400 Ω/□ (200 °C) at the annealing time of 15 min. However, samples demonstrated different behaviors upon increasing the annealing time to 30, 60 and 120 min. Upon increasing the time to 30 min, the sheet resistance of the films annealed at 100 and 125 °C decreased to 53 Ω/□ and 18.3 Ω/□, respectively and then leveled off. On the other hand, the sheet resistance of the sample annealed at 150 °C increased progressively with the annealing time. However, the sheet resistance of the sample annealed at 200 °C increased sharply upon increasing the time to 30 min and henceforth no measurements could be taken.

The topology of the annealed 6 bilayer AgNW samples was investigated by FE-SEM to obtain a better understanding on the change of sheet resistance upon thermal treatment. It can be deduced that the CA and MPA were fully removed from the nanowire surface and the AgNWs fused into each other at the junctions by annealing at 125 °C (Figure 3.8b). The successful removal of the capping agents was proven by XPS characterization (not shown here). The higher sheet resistance at 100 and 150 °C could be explained by the partial removal of the capping agents and slightly over melting of the AgNWs, respectively. However, annealing at 200 °C provided large island-type particles and shorter nanowires (Figure 3.8c) due to the over melting of the AgNWs and high surface tension of melted silver. Hence, the optimum annealing condition was found as 125 °C and 30 min, which provided sheet resistance of 18.3 Ω/□ that is comparable to commercial ITO electrode (Rs = 15.3 Ω/□) [79].

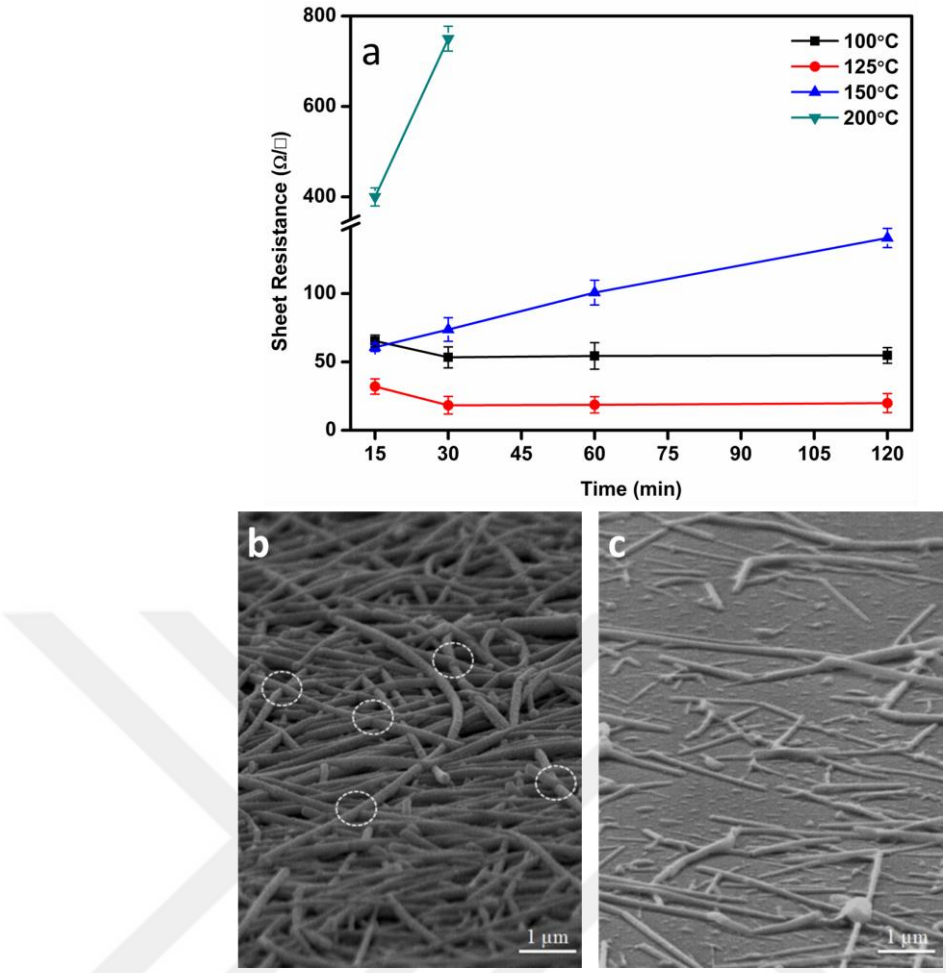

Figure 3.8 : (a) Sheet resistance vs. annealing time behaviors of 6-bilayer AgNW film for different temperatures between 100 and 200 °C in air. Tilted SEM images of 6-bilayer AgNW film annealed (b) at 125 °C for 30 min and (c) at 200 °C for 30 min.

Unlike the typical annealing at 200–250 °C of PVP capped AgNWs in the literature [81,82], LBL assembled filmrequired annealing temperature of 125 °C. This could be attributed to the low molecular weight of CA (113.61 g/mol) and MPA (106.14 g/mol) which in turn led to low temperature decomposition when compared to PVP (~55.000 g/mol). In addition, the sheet resistance was investigated as a function of layer number asdepicted in Figure 3.9. One and two bilayer samples provided very high sheet resistance (~10^5–10^6 Ω/□), which could be explained by incomplete electrically conductive network formation (Figure 3.6a). However, increasing the layer number to five bilayers resulted in a linear decrease of the sheet resistance, demonstrating the successful insulator-conductor transition. This could be attributed to the increased number of nanowires and formation of new conductive pathways (Figure 3.6b, c). In addition, extending the layer number (N5) does not have significant effect on the sheet resistance.

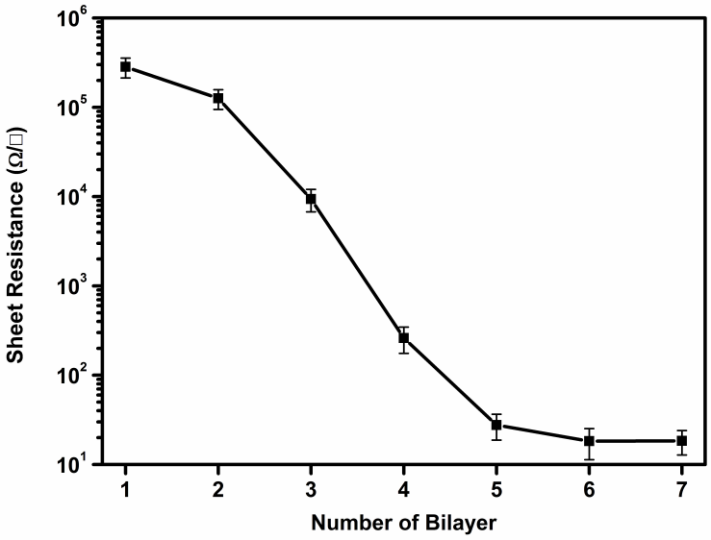

Figure 3.9 : Sheet resistance of LBL assembled AgNW films as a function of number of bilayer.

Moreover, the sheet resistance and optical transmittance at 550 nm values were utilized to evaluate the performance of AgNW films by calculating the figure of merit (Φ_{TC}) via Haacke equation [43];

$\Phi_{TC} = T^{10}/R_s$

where T is the optical transmittance at 550 nm and R_s is the sheet resistance (Table 3.1). The higher is the value of the figure of merit, the better is the performance of a TCE. In this work, best performance was obtained with 6-bilayer film (9.33×10^{-3} Ω^{-1}), which is even higher than that of the sputtered ITO film (6.6×10^{-3} Ω^{-1}), indicating the possible use of LBL assembled AgNWs as an alternative for ITO (T=79.5%, Rs= 15.3 Ω/□) [79].

Table 3.1 : The optical transmittance, sheet resistance and figure of merit values of LBL assembled AgNWs films.

Number of bilayers	T (%)	R_s (Ω/□)	ϕ_{TC} (10^{-3} Ω^{-1})
1	97.8	284×10^3	0.0028
2	95.9	126×10^3	0.0052
3	93.8	9.4×10^3	0.056
4	90.1	261	1.35
5	85.9	27.7	7.90
6	83.8	18.3	9.33
7	80.6	18.4	6.28

Consequently, 6-bilayer AgNW film performance was compared with the previous works in Figure 3.10. The comparison reveals that our work provided better performance than films fabricated by rod coating, spray coating and spin coating. This could be attributed to the difficulties in obtaining uniform films and loose packing density of the nanowires with those methods. Conversely, vacuum filtration and drop coating methods provided higher figure of merit values ($22.27 \times 10^{-3}\ \Omega^{-1}$) than our work, which may be explained by the higher packing density of AgNWs due to the applied vacuum (in vacuum filtration) or slow drying of the solvent (in drop coating). Nevertheless, these two methods are not scalable and it is a real challenge to coat large area samples.

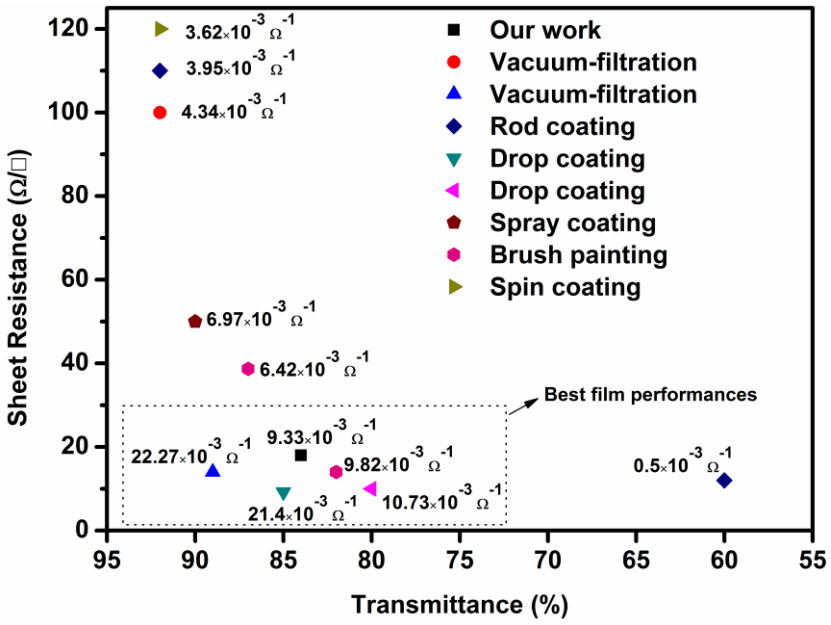

Figure 3.10 : Comparison of the sheet resistance and optical transmittance values of the present study with the references.

Moreover, the films obtained by the above-mentioned methods have weak adhesion, because there is no interaction between the substrate and the AgNWs. Adhesion of the AgNWs to the substrate is a critical problem, because it influences the long-term utilization of the electrode in the optoelectronic devices. Typically, the AgNW multilayer films in this work easily passed adhesion test with 3-M tapes without any change in sheet resistance and topology (not shown here). This could be explained by the presence of APTES molecules (b.p. 217 °C) on the substrate even after annealing process. The amine groups are well known to have strong affinity to silver atoms, which enhances the adhesion of AgNWs to the substrate.

Finally, conductivity of the 6-bilayer film was also visually demonstrated in Figure 3.11. The sample was connected to the electrodes of a printed circuit board to which a voltage (~3 V) is applied. 30mA current passed through the AgNW film, which lid the LED successfully.

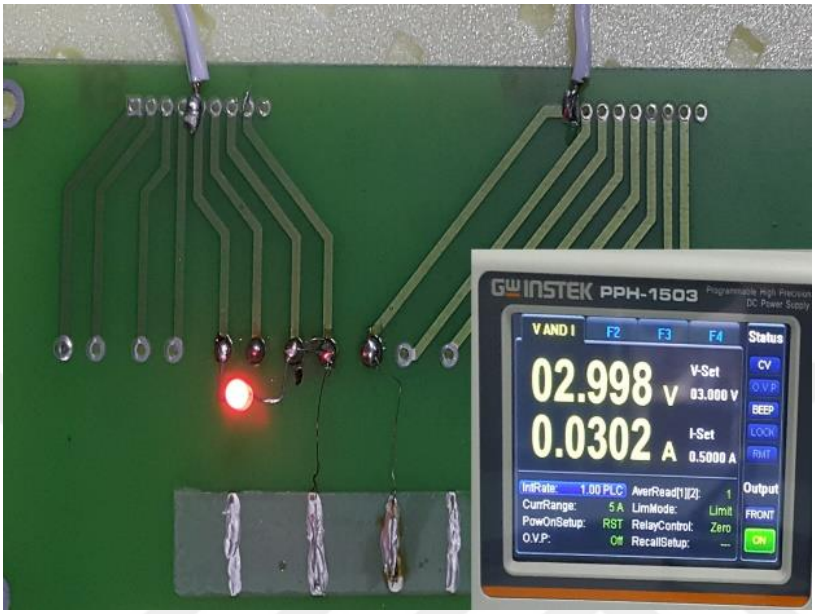

Figure 3.11 : Passing current through 6-bilayer AgNW coated glass substrate to power a LED (Inset demonstrates the voltage and current of the system).

3.3 Conclusion

In summary, high performance TCE was successfully prepared via LBL assembly of AgNWs in this work. Carboxylic acid and amine moieties were introduced on the nanowires via ligand exchange process. LBL assembly was successfully implemented with the negatively and positively charged AgNWs as confirmed by the decreased optical transmittance and sheet resistance. Optimum annealing conditions was found as 125 °C and 30min which was evaluated by sheet resistance measurement. The highest figure of meritwas evaluated as $9.33\times 10^{-3}\ \Omega^{-1}$ at 83.8% optical transmittance for 6-bilayer film, which powered the LED upon applying voltage.

4. COUPLING LAYER-BY-LAYER ASSEMBLY AND MULTILAYER TRANSFER TO FABRICATE FLEXIBLE TRANSPARENT FILM HEATER [1]

Recently, flexible transparent film heaters (f-TFHs) have attracted considerable attention in various applications, including defrosters, displays, solar panels, touch screens, wearable devices and sensors [83]. The principle of f-TFHs is based on Joule heating, which converts electricity to heat [84]. Thermal response time, steady-state temperature, temperature uniformity and stability are the essential issues for f-TFHs. High optical transmittance and low sheet resistance are the other most crucial parameters to determine the performance of f-TFHs.

Transparent conductive electrode (TCE) with high conductivity and transparency is the key component for f-TFHs [85-87]. High optical transmittance makes the transparent heaters suitable for various applications where clear visibility is required, such as vehicle window, while low sheet resistance is required not only for rapid heating but also for maintaining high saturated temperature under low input power [88]. Therefore, both optical transmittance and sheet resistance have to compromise with each other.

Indium tin oxide (ITO) has been widely used to fabricate f-TFHs in industry [89], due to its excellent optoelectronic properties [90,91]. However, it has many drawbacks such as the increasing price of indium source, brittleness, instability in acid or basic mediums, lack of flexibility and high production costs [92,93]. Many alternative conductive materials have been offered to fabricate f-TFHs such as hybrid materials, silver nanowires (AgNWs), copper nanowires, carbon nanotubes and graphene [89,94-100]. Among them, AgNWs have been considered the best candidate due to their excellent optoelectrical properties and high flexibility [101,102]. Up to date, f-TFHs have been generally fabricated on polyethylene terephthalate (PET) substrate because PET has many advantages such as high flexibility, transparency and low cost. However, the relatively low glass transition

[1] This chapter is based on the paper " Oytun F., Alpturk O., and Basarir F., Coupling layer-by-layer assembly and multilayer transfer to fabricate flexible transparent film heater. Materials Research Bulletin, 2019, 112, 53-60."

temperature of PET (T_g: 67-81 °C) limits the maximum temperature that the AgNW-based f-TFHs can reach [103].

Variety of solution based coating methods were offered in the literature to prepare flexible AgNW films, such as drop-casting, spray coating, brush painting, spin coating and meyer-rod-coating [9,84,104-106]. The mentioned methods are low-cost techniques compared with the conventional vacuum deposition for ITO production [107]. In addition, they provide TCEs with low sheet resistance and high optical transmittance. However, the difficulties in large area coating and the challenges in obtaining uniform films are the significant disadvantages of these techniques [59]. Moreover, large amounts of waste material after coating and the problems in viscosity adjustments are other major drawbacks of mentioned methods.

On the other hand, layer-by-layer (LBL) deposition is a very promising approach consisting of sequential immersion of a substrate into aqueous solutions of oppositely charged materials [108-111]. This method can create versatile thin films with highly tunable thickness, porosity, packing density and surface properties [60]. Furthermore, the multilayer film has excellent adhesion to the substrate since the multilayer is formed via covalent bonding or ionic interaction [61]. Thus, it has been widely utilized for fabrication of solution processed polymer and nanomaterial multilayer films for various applications [112-116].

Therefore, to address this issue, in this study, we fabricated flexible, transparent and conductive AgNW films on highly thermal stable polysulfone (PSU) film via layer-by-layer assembly (LBL) of functional AgNWs for use in f-TFHs application. First, amine and carboxylic acid groups were grafted on AgNWs to obtain positively and negatively charged AgNWs, respectively. Then, LBL deposition of oppositely charged AgNWs was achieved on glass substrates via ionic interaction between amine and carboxylic acid groups, resulting in uniform network. Next, thermal annealing was applied to increase the conductivity of films, followed by drop casting PSU solution over LBL assembled AgNW film on glass substrate and waited for solvent evaporation. The resulting film was peeled off on the glass substrate. Finally, optoelectronic, thermal, morphological and mechanical performance of the films were evaluated.

4.1 Experimental

4.1.1 Materials

Silver nanowires (AgNWs) were purchased from ACS Materials (USA) as suspension in isopropyl alcohol (IPA) with a concentration of 20 mg/ml. The average length and diameter of the AgNWs were 20-30 μm and 60 nm, respectively. Cysteamine hydrochloride (CA, BioXtra), 3-mercaptopropionic acid (MPA, 99%), 3-aminopropyltriethoxysilane (APTES, 99%), N,N-dimethylformamide (DMF, 99.8%) and dichloromethane (DCM, ≥ 99.8%, b.p.: 40 °C) were obtained from Sigma–Aldrich. Polysulfone (PSU, MW: 29,000 g/mol) was provided by Solvay Advanced Polymers. Microscope slides (ISOLAB) with dimensions of 76x26x1 mm were used as glass substrate. All aqueous solutions were prepared with the deionized water (DI, 18.2 MΩ) with a Millipore-Q system.

4.1.2 Methods

Amine (AgNW-NH_2) and carboxylic acid (AgNW-COOH) functionalized silver nanowires were prepared based on our previous report [101]. Prior to the coating, the glass substrates were ultrasonically cleaned in acetone and ethanol for 10 min and dried with pure N_2 flow. Then, they were treated with O_2 plasma for 60 s at 50 W to generate hydroxyl groups on the surface. Afterwards, the substrates were dipped in 3% (v/v) APTES solution in ethanol for 2 h to create amine groups on the surface, followed by rinsing vigorously with ethanol and annealing in an oven at 120°C for 1 h.

The layer-by-layer (LBL) coatings were performed by using an automatic slide stainer (Sakura DRS-2000) on APTES modified glass substrates. First, the substrates were immersed into negatively charged AgNW-COOH solution for 15 min, followed by rinsing with DI water and blow-drying with hot air. Then, the substrates were immediately immersed into positively charged AgNW-NH_2 solution for 15 min. The substrates were again rinsed with DI water and blow-dried with hot air. The multilayer films were simply prepared by repeating these processes. The films were subsequently annealed at 125 °C for 30 min in a tube furnace under air atmosphere to increase the electrical conductivity.

To obtain flexible thin film heater (f-TFH), PSU (50 mg/ml) dissolved in DCM was dropped over the AgNW multilayer film and waited until the solvent was evaporated.

Consequently, the PSU film was peeled off from the glass substrate which led to full transfer of AgNW multilayer to the PSU film.

4.1.3 Characterization

The sheet resistance measurements were performed by using 4-point probe (Everbeing SR-4) whereas the optical transmission was measured with UV-Vis spectrometer (Lambda 750, Perkin Elmer). Field emission scanning electron microscope (FE-SEM, JEOL JSM-6500F) and optical microscope (Axio Scope A1, Zeiss) were used to investigate the surface morphology of the films.

The performance of the f-TFH was evaluated by using an infrared thermal imager (Flir SC4000). In order to heat the film, DC voltage was applied through silver contacts at the edges using a power supplier (GW Instek PPH 1503). The bending test was performed by directly bending the film to 90° manually by hand. For the defrosting tests, f-TFH was placed into a fridge for 30 min to form frost on the entire film, followed by applying voltage (3~7 V) to the film. The adhesion test was carried out by 3M scotch tape. The tape was fully adhered on the AgNW films and then detached after 30 s. The process was repeated up to 20 detachments and the sheet resistance of film was recorded after each 5 detachments.

4.2 Results and Discussion

Fabrication of f-TFH was schematically illustrated in Figure 4.1. First, LBL assembly was performed via electrostatic interaction between the AgNW-NH_2 and AgNW-COOH on glass substrates. Then, the PSU solution was drop-cast onto the LBL assembled AgNW film and waited for solvent evaporation. Then, the resulting film was easily peeled off from the glass substrate. The entire AgNW film was fully transferred from the glass to the PSU substrate leaving no residue on the glass substrate.

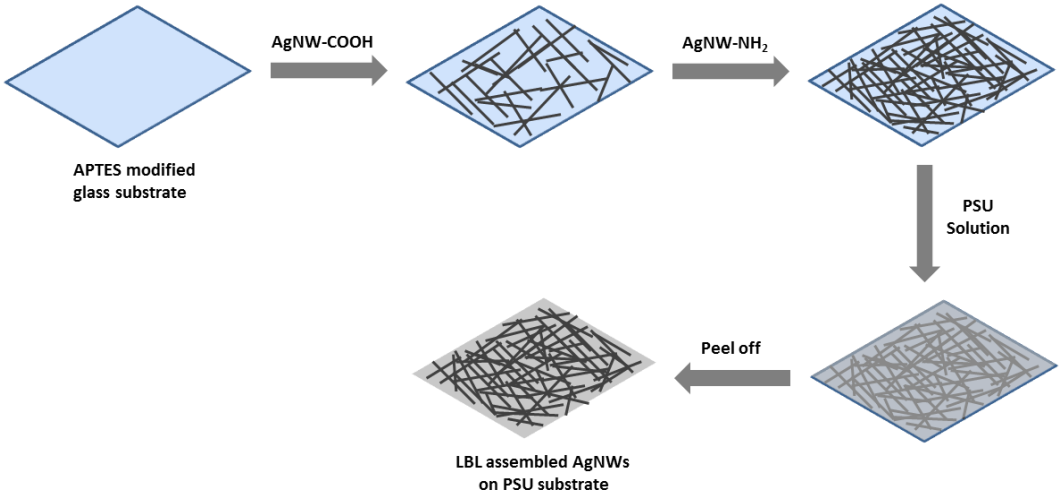

Figure 4.1 : Schematic illustration of LBL assembly and fabrication of AgNW films on PSU.

Figure 4.2 shows the optical microscope images of AgNW films with different bilayer numbers. It is clear that the AgNW coverage increases stepwise with the increase of the bilayer number, demonstrating the successful LBL deposition. 5 bilayer sample demonstrates dense and uniform AgNW network on the surface, which provides electrical pathways throughout the entire network and effective percolative network. In addition, low roughness and smoother surface may also be required for various practical applications. It is worthy to note that cold pressing can help to obtain smoother surface after multilayer transfer of AgNWs onto flexible substrate. Therefore, cold pressing was applied to the AgNW film at 20 MPa for 15 s. The AFM results (not shown here) reveals that the RMS roughness decreased from 58 nm to 42 nm upon cold pressing. The similar phenomenon was observed by Lan et.al [84].

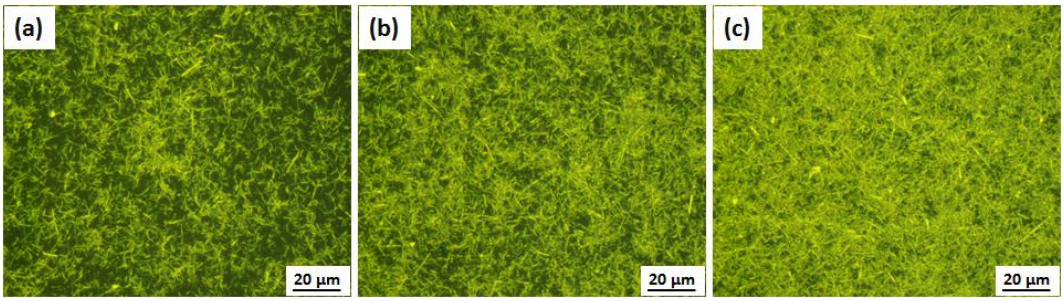

Figure 4.2 : Optical microscope images of AgNW films on PSU; (a) 1 bilayer, (b) 3 bilayer and (c) 5 bilayer

Figure 4.3a shows the optical transmittance of films in the visible region. The optical transmittance decreases with the number of bilayers, which again indicates the successful LBL deposition. The transmittances at 550 nm were measured as 95, 89 and 84% for 1, 3 and 5 bilayer, respectively. On the other hand, the sheet resistances of films decreased with increasing bilayer number, as shown in Figure 4.3b. The sheet resistances were found as ~5000, 90 and 12 Ω/□ for 1, 3 and 5 bilayer, respectively. Figure 4.3c shows the macro images of films, which displays their transparency. It is clearly shown that the film is still very transparent even after 5 bilayer deposition. The results reveal that the 5 bilayer film can be an alternative for ITO (T: 80%, R_s: 15 Ω/□) [101].

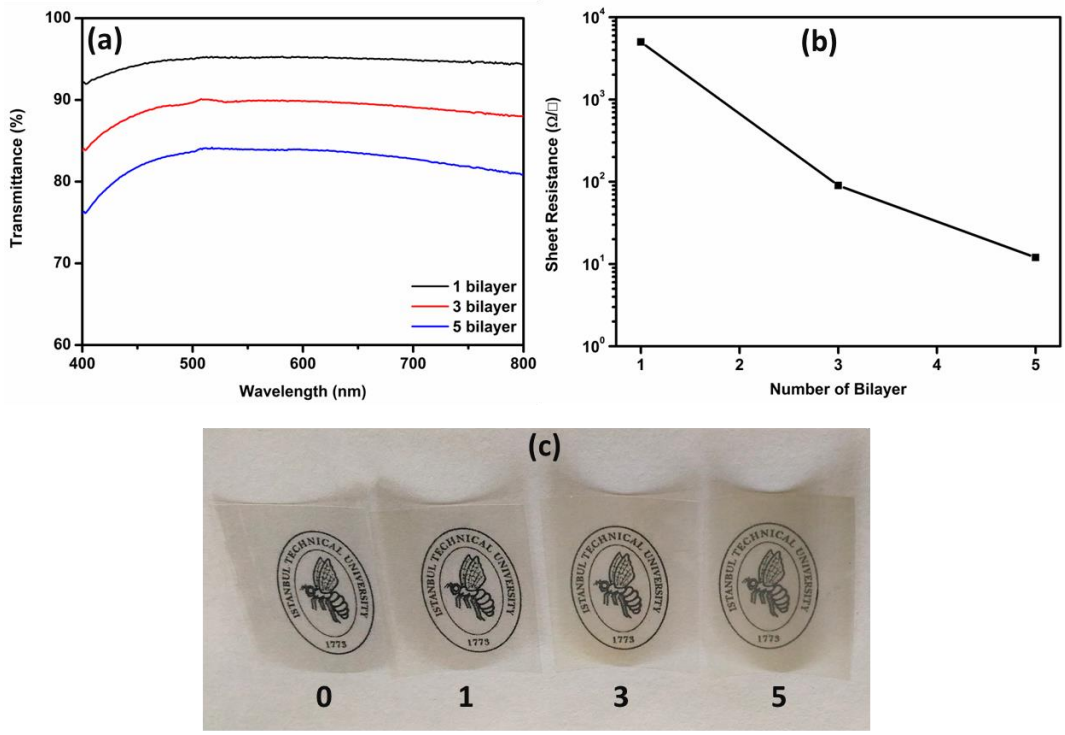

Figure 4.3 : (a) Optical transmittance, (b) Sheet resistance and (c) macro images of AgNW multilayer films on PSU.

The adhesion between AgNWs and PSU was investigated by 3M Scotch tape tests, which was applied on the surface of films simply by hand. Figure 4.4a gives the sheet resistance change of AgNW film with peeling by tape. Significant change was not observed in the sheet resistance of 5-bilayer film even after 20 peeling cycle, indicating the strong interaction between AgNW network and PSU film. This interaction may be attributed to the strong hydrogen bonding between the sulfonic groups of PSU and amine groups of AgNW-NH_2, as shown in Figure 4.4b [40].

Besides, the film demonstrated excellent flexibility without losing conductivity even after 300 times bending (Figure 4.4c).

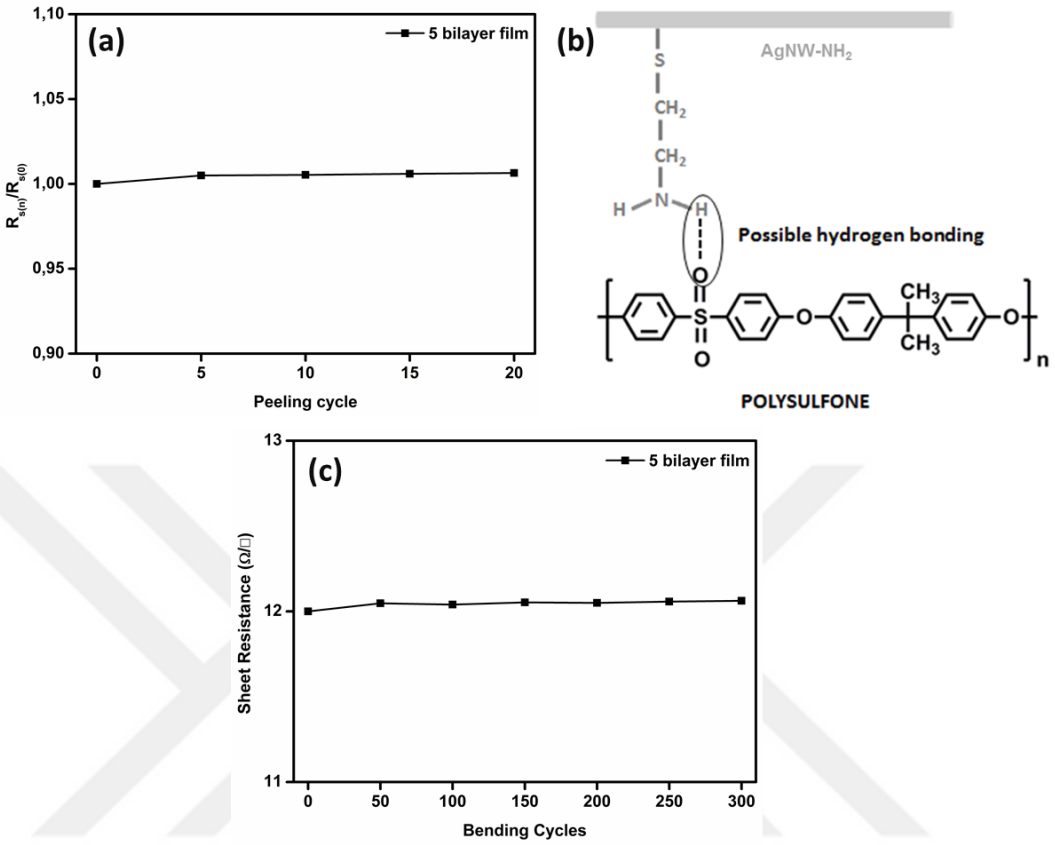

Figure 4.4 : (a) Sheet resistance changes of AgNW film after repeated adhesion and peeling cycles, (b) Possible hydrogen bonding between the sulfonic groups of PSU and amine groups of AgNW-NH_2 and (c) Sheet resistance values of AgNW film with the bending cycles.

Schematic illustration of fabricated f-TFHs was shown in Figure 4.5a. The DC voltage was applied to film heaters through silver contact at the film edges and the temperature of the film was monitored using an IR thermal imager. Figure 4.5b displays the change in temperature of the film heaters with different bilayer numbers at 6 V constant voltage for 150 s. Upon turning on the DC voltage supplier, the temperature rapidly increased and then saturated after a while for all films, whereas sudden decreases of the temperature were observed after switching off. The films with 1, 3 and 5 bilayer reached to the highest temperature about 24, 74 and 95 °C, respectively. The response time, which is defined as the time required to reach saturation temperature, is one of important parameters for evaluating the performance of film heaters [117]. The response times were observed as 10, 20 and 35 s, respectively. This trend is accordance with a study published by Li et al [103].

Figure 4.5c shows the temperature profiles of the 5 bilayer sample with respect to the applied voltages. DC voltages of 3, 4, 5, 6 and 7 V were sequentially applied to the f-TFH. The generated temperature of the film heater increased with increasing the voltage and the temperature was measured as 128 °C with 7 V. On the other hand, the response time was found as 45 s, demonstrating the fast response of the device. These results strongly suggest that AgNW film with 5 bilayer is suitable for transparent heaters such as window defrosters in cars or buildings [118].

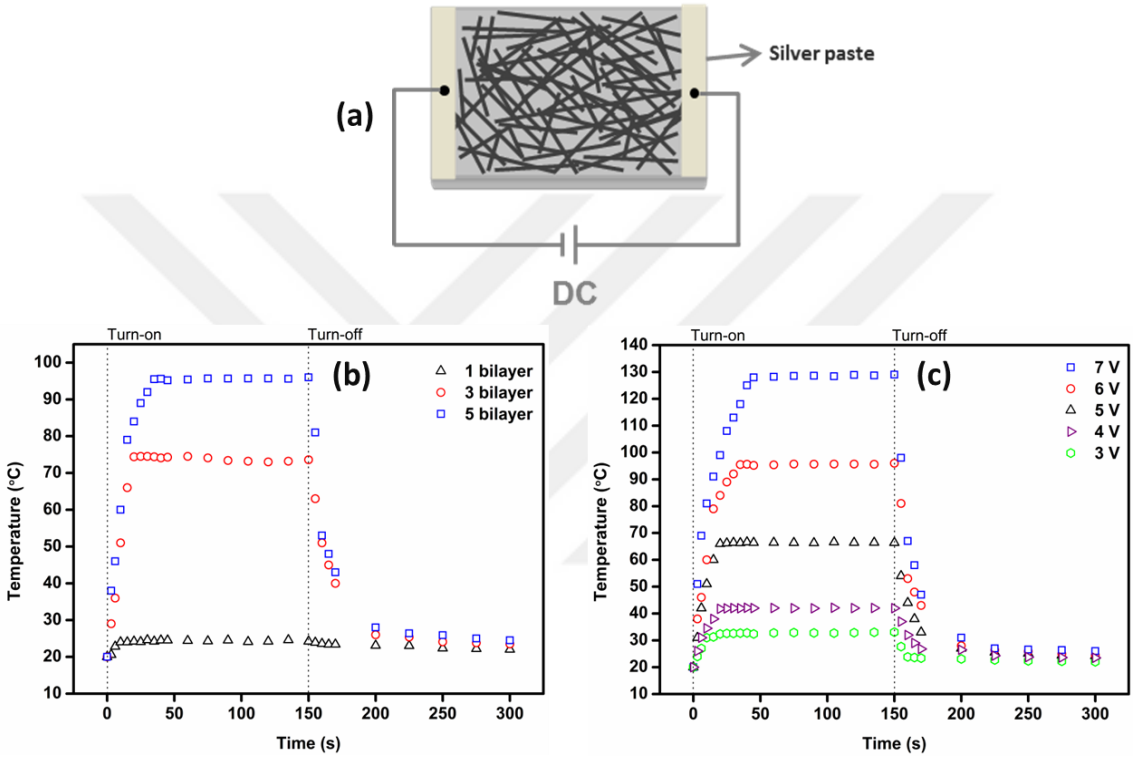

Figure 4.5 : (a) A schematic illustration of film heater. (b) The temperatures of films at 6V constant voltage and (c) Measured temperatures for film with 5 bilayer at different voltages.

Figure 4.6 presents the infrared thermal images of fabricated AgNW films. The all images clearly show that the temperature distributions are quite uniform over the entire film. Figure 4.6a-c displays thermal images of films with different bilayers at 6 V. At the same input voltage, the maximum temperature increases as the bilayer number of the films increases. The temperature increased to 95 °C for 5 bilayer, whereas it reached to 24 °C for 1 bilayer when constant voltage of 6 V was applied (R.T: 19°C). The increase in temperature is due to the efficient transduction of electrical energy into Joule heating, which may be attributed to the improved conductivity of the AgNW film [95].

On the other hand, the effect of voltages on temperature distribution of 5 bilayer film was investigated in Figure 4.6d-f. By increasing the voltage from 3 to 7 V, the thermal images became more orange, indicating the increase of temperature. The temperature reached to 128 °C when 7 V was applied, while it was 32 °C at 3 V. Therefore, the same film heater could be used to meet different temperature requirements by simply applying an appropriate voltage. These results show that the AgNW films are promising candidates for transparent film heater that require uniform heating temperature.

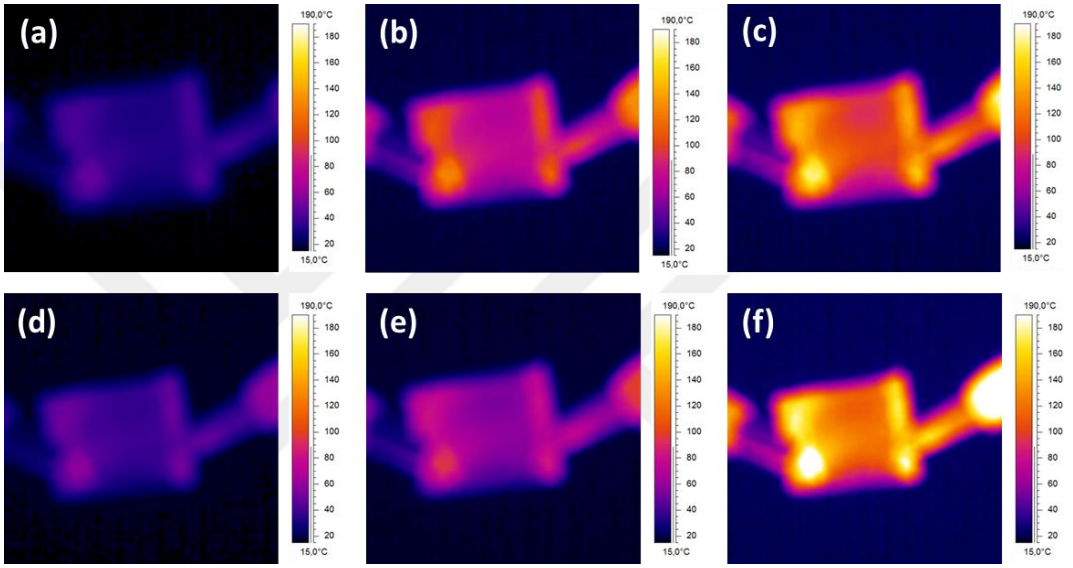

Figure 4.6 : Infrared (IR) thermal images of AgNW films with (a) 1 bilayer, (b) 3 bilayer, (c) 5 bilayer film at 6 V constant voltage and IR thermal images of 5 bilayer film at (d) 3 V, (e) 5 V and (f) 7 V.

Long-term working stability of f-TFH is the one of most important factors in practical applications [103]. Figure 4.7 shows output temperature when 7 V was applied continuously for 5 h to the 5 bilayer film. The generated temperature slightly decreased from 128 °C to 125 °C at the end of 5 hours period, which can be explained by little structure degradation of AgNW network. Except for these changes, Fig. 7 confirms that the film shows a stable heating performance for a long heating time. In addition, the transmittance of film remained unchanged after this long heating process.

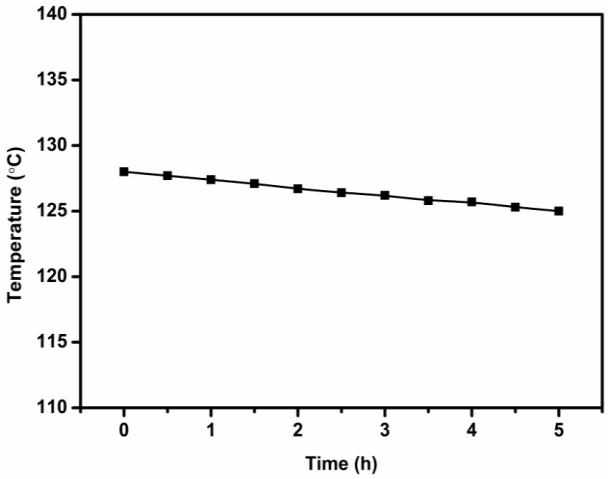

Figure 4.7 : Working stability of 5 bilayer film by applying 7 V for 5 h.

Figure 4.8 shows the SEM images of AgNW film with 5 bilayer before and after applying different voltages for 5 hours. As can be seen from Figure 4.8a and 4.8b, the AgNW network remained undisrupted when 7 V was applied for 5 h. However, by increasing the voltage to 8 V, the film heater reached quickly a temperature of 175 °C and the temperature decreased suddenly up to initial temperature after a short time. The decrease in temperature is due to the electrical breakdown, resulting in disruption of AgNW network, as shown in Figure 4.8c. A similar phenomenon was observed by Cheong et al [119].

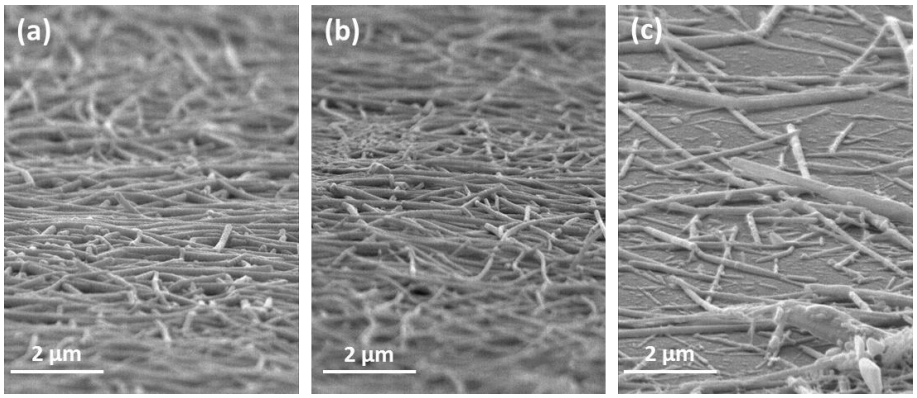

Figure 4.8 : SEM images of AgNW films with 5 bilayer (a) before, (b) after applying voltage of 7 V and (c) 8 V for 5 h.

Transparent film heaters fabricated on PET have been reported previously to obtain flexible film heaters. The relatively low glass transition temperature of PET prevents reaching high temperature values. However, PSU with high thermal resistance due to its high glass transition temperature overcomes this problem [92]. The maximum temperature evaluated (128 °C) in this work is higher than the ones in the literature

as shown in Table 4.1. This can be explained by the higher heat resistance of PSU. However, the AgNW network in our study begins to deteriorate when the temperature is higher than 128 °C. Normally, typical PVP capped AgNWs are thermally stable up to 200-250 °C. The thermal stability of CA and MPA capped AgNWs decreased after the ligand exchange of AgNWs with CA and MPA. As emphasized in our previous work [101], the reduced thermal stability could be attributed to the low molecular weight of CA (113.61 g/mole) and MPA (106.14 g/mole) which led to low thermal decomposition when compared to PVP (~55.000 g/mole).

Table 4.1 : Properties of transparent film heaters fabricated in the literature

Materials	**Rs (Ω/□)**	**T%**	**T_{max} (^{o}C)**	**V_{input} (V)**	**Ref.**
Current Material (ITO)	392	95.6	31.4	12	89
CNT/AgNW	30	95	110	15	89
AgNW	10	90	105	7	94
AgNW	15	61	48	-	95
AgNW/PEDOT:PSS	3	83	86	3	96
CuNW	17-96	84-91	120	5	97
SWCNT	580	79	95	12	98
MWCNT	349	72	65	12	99
Doped graphene	43	80	97	12	100

On the other hand, the f-TFH was tested to demonstrate its potential as an efficient defroster (Figure 4.9). The film was initially put in a refrigerator for 30 min to generate frost on the film surface. The transparency of the PSU disappeared due to the formation of frost on the film, as shown in Figure 4.9b. The frost was completely removed on the film surface when 7 V was applied for 20 s and original visibility was recovered (Figure 4.9c).

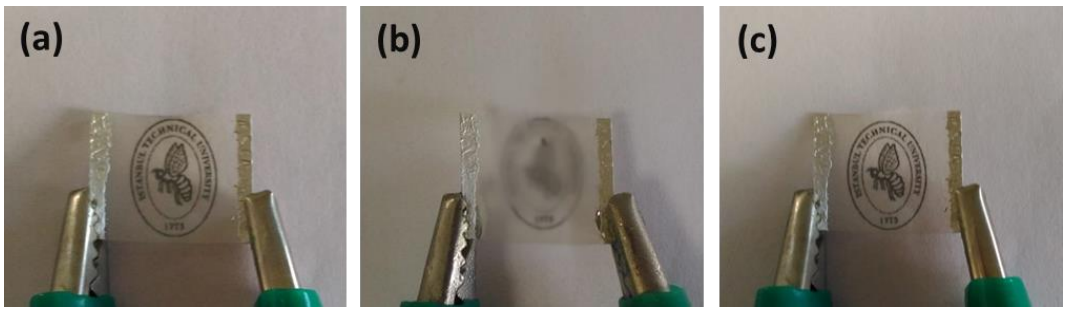

Figure 4.9 : Defrosting test photographs of the film heater with 5 bilayer; (a) before (b) frosted film heater and (c) the film heater after applying voltage of 7 V for 20 s.

4.3 Conclusion

In this study, an efficient flexible transparent conductive AgNW films on PSU was fabricated via layer by layer assembly of functional AgNWs. 5 bilayer films showed superior optoelectronic properties in terms of transparency and sheet resistance. In addition, adhesion and bending tests showed that AgNW film had strong bonding force between AgNWs and PSU and high mechanical flexibility, respectively. In addition, the film heater exhibited rapid thermal response time (45 s) and thermal stability for 5 h at 128 °C. We believe that the AgNW films on PSU film is not limited to f-TFH and can be used in various applications requiring good optoelectronic, high mechanical flexibility and thermal properties.

5. CONCLUSIONS

Although ITO with good optoelectronic properties has dominated the TCE market, which is a widely used in OLED, OPVs, film heaters, touch screen applications, it has several drawbacks such as high costs and brittle nature. Therefore, there is a growing need to alternative materials instead of ITO. For this purpose, in this thesis, transparent conductive electrodes as an alternative to ITO have fabricated on glass or flexible substrate via layer by layer method using functional nanomaterials such as different types of carbon nanotubes and silver nanowires. Higly transparent and conductive electrodes have exhibited good optoelectronic properties and film thicknesses can be easily tuned by low cost layer by layer method. In addition, the electrodes fabricated in this thesis have founded compatible with flexible applications, which is restricted by ITO.

In the first part of this thesis, flexible transparent conductive CNT films prepared by LBL method were successfully transferred on flexible polymer substrate. The LBL method provided us desired optical transmittance values for CNT films. The sheet resistances of films were improved using chemical and thermal post treatments. Flexible films were obtained by solvent casting of PSU solution, followed by peeling off from glass substrate. The multilayered flexible films were demonstrated the unchanged transmittance and conductivity. Especially, flexible SWCNT films exhibited reasonable optoelectronic properties compared with commercial ITO. The films were finally tested in resistive touch sensor application.

The second part of this thesis describes the fabrication of highly transparent and conductive AgNW electrodes on glass substrate via LBL deposition. LBL assembled AgNW films were prepared for the first time using our approach. In the novel method, AgNWs were functionalized with some functional groups carrying negative and positive charge. The opposite charges on the AgNW surface provided good ionic interaction in the coating process. The films were exhibited excellent optoelectronic properties. Finally, the conductivity of multilayered film was demonstrated in an application, which powered the LED upon applying a voltage.

The last part in this thesis describes fabrication of flexible transparent AgNW films and its application in film heater. Optoelectronic properties of flexible films were

better than that of commercial ITO. The films were prepared as a flexible transparent film heater and its thermal properties were extensively characterized. The film heater showed superior mechanical and thermal properties. Even after 300 bending cycles, the films protected its optoelectronic and thermal properties. The f-TFH reached maximum temperature of 128 °C and showed stable heating for 5 h.

It is believed that the concepts presented here will open new pathways to further developments of transparent conductive electrodes for various optoelectronic applications.

REFERENCES

[1]. **Meng, Y., Xu, X.-B., Li, H., Wang, Y., Ding, E.-X., Zhang, Z.-C., and Geng, H.-Z.** (2014). Optimisation of carbon nanotube ink for large-area transparent conducting films fabricated by controllable rod-coating method. *Carbon*, *70*, 103–110.

[2]. **Zhang, D., Ryu, K., Liu, X., Polikarpov, E., Ly, J., Tompson, M. E., and Zhou, C.** (2006). Transparent, conductive, and flexible carbon nanotube films and their application in organic light-emitting diodes. *Nano Letters*, *6*, 1880–1886.

[3]. **Gomez De Arco, L., Zhang, Y., Schlenker, C. W., Ryu, K., Thompson, M. E., and Zhou, C.** (2010). Continuous, Highly Flexible, and Transparent Graphene Films by Chemical Vapor Deposition for Organic Photovoltaics. *ACS Nano*, *4*, 2865–2873.

[4]. **Chen, Z., Cotterell, B., and Wang, W.** (2002). The fracture of brittle thin films on compliant substrates in flexible displays. *Engineering Fracture Mechanics*, *69*, 597–603.

[5]. **Sierros, K. A., Morris, N. J., Ramji, K., and Cairns, D. R.** (2009). Stress–corrosion cracking of indium tin oxide coated polyethylene terephthalate for flexible optoelectronic devices. *Thin Solid Films*, *517*, 2590–2595.

[6]. **Kymakis, E., Stratakis, E., and Koudoumas, E.** (2007). Integration of carbon nanotubes as hole transport electrode in polymer/fullerene bulk heterojunction solar cells. *Thin Solid Films*, *515*, 8598–8600.

[7]. **Kymakis, E., Stratakis, E., Stylianakis, M. M., Koudoumas, E., and Fotakis, C.** (2011). Spin coated graphene films as the transparent electrode in organic photovoltaic devices. *Thin Solid Films*, *520*, 1238–1241.

[8]. **Ji, T., Tan, L., Bai, J., Hu, X., Xiao, S., and Chen, Y.** (2016). Synergistic dispersible graphene: Sulfonated carbon nanotubes integrated with PEDOT for large-scale transparent conductive electrodes. *Carbon*, *98*, 15–23.

[9]. **Hu, L., Kim, H. S., Lee, J. Y., Peumans, P., and Cui, Y.** (2010). Scalable coating and properties of transparent, flexible, silver nanowire electrodes. *ACS Nano*, *8*, 2955–2963.

[10]. **Gruner, G.** (2006). Carbon nanotube films for transparent and plastic electronics. *J. Mater. Chem.*, *16*, 3533–3539.

[11]. **Jung, D., Lee, K. H., Kim, D., Burk, D., Overzet, L. J., and Lee, G. S.** (2013). Highly Conductive Flexible Multi-Walled Carbon Nanotube Sheet Films for Transparent Touch Screen. *Japanese Journal of Applied Physics*, *52*, 03BC03.

[12]. **Salvatierra, R. V, Cava, C. E., Roman, L. S., and Zarbin, A. J. G.** (2013). ITO-Free and Flexible Organic Photovoltaic Device Based on High Transparent and Conductive Polyaniline/Carbon Nanotube Thin Films. *Advanced Functional Materials*, *23*, 1490–1499.

[13]. **Kymakis, E., and Amaratunga, G. A. J.** (2002). Single-wall carbon nanotube/conjugated polymer photovoltaic devices. *Applied Physics Letters*, *80*, 112–114.

[14]. **Cho, D.-Y., Eun, K., Choa, S.-H., and Kim, H.-K.** (2014). Highly flexible and stretchable carbon nanotube network electrodes prepared by simple brush painting for cost-effective flexible organic solar cells. *Carbon*, *66*, 530–538.

[15]. **Chien, Y.-M., Lefevre, F., Shih, I., and Izquierdo, R.** (2010). A solution processed top emission {OLED} with transparent carbon nanotube electrodes. *Nanotechnology*, *21*, 134020.

[16]. **Paul, S., and Kim, D.-W.** (2009). Preparation and characterization of highly conductive transparent films with single-walled carbon nanotubes for flexible display applications. *Carbon*, *47*, 2436–2441.

[17]. **Sierros, K. A., Hecht, D. S., Banerjee, D. A., Morris, N. J., Hu, L., Irvin, G. C… Cairns, D. R.** (2010). Durable transparent carbon nanotube films for flexible device components. *Thin Solid Films*, *518*, 6977–6983.

[18]. **Scardaci, V., Coull, R., and Coleman, J. N.** (2010). Very thin transparent, conductive carbon nanotube films on flexible substrates. *Applied Physics Letters*, *97*, 23114.

[19]. **Rahy, A., Bajaj, P., Musselman, I. H., Hong, S. H., Sun, Y.-P., and Yang, D. J.** (2009). Coating of carbon nanotubes on flexible substrate and its adhesion study. *Applied Surface Science*, *255*, 7084–7089.

[20]. **Ng, M. H. A., Hartadi, L. T., Tan, H., and Poa, C. H. P.** (2008). Efficient coating of transparent and conductive carbon nanotube thin films on plastic substrates. *Nanotechnology*, *19*, 205703.

[21]. **Lima, M. D., de Andrade, M. J., Bergmann, C. P., and Roth, S.** (2008). Thin{,} conductive{,} carbon nanotube networks over transparent substrates by electrophoretic deposition. *J. Mater. Chem.*, *18*, 776–779.

[22]. **Kim, B.-J., Park, J.-S., Hwang, Y.-J., and Park, J.-S.** (2015). Characteristics

of silver meshes coated with carbon nanotubes via spray-coating and electrophoretic deposition for touch screen panels. *Thin Solid Films*, *596*, 68–71.

[23]. **Tenent, R. C., Barnes, T. M., Bergeson, J. D., Ferguson, A. J., To, B., Gedvilas, L. M… Blackburn, J. L.** (2009). Ultrasmooth, Large-Area, High-Uniformity, Conductive Transparent Single-Walled-Carbon-Nanotube Films for Photovoltaics Produced by Ultrasonic Spraying. *Advanced Materials*, *21*, 3210–3216.

[24]. **Imazu, N., Fujigaya, T., and Nakashima, N.** (2014). Fabrication of flexible transparent conductive films from long double-walled carbon nanotubes. *Science and Technology of Advanced Materials*, *15*, 25005.

[25]. **Wang, Y., Yang, H.-J., Geng, H.-Z., Zhang, Z.-C., Ding, E.-X., Meng, Y… Da, S.-X.** (2015). Fabrication and evaluation of adhesion enhanced flexible carbon nanotube transparent conducting films. *J. Mater. Chem. C*, *3*, 3796–3802.

[26]. **Abdelhalim, A., Abdellah, A., Scarpa, G., and Lugli, P.** (2013). Fabrication of carbon nanotube thin films on flexible substrates by spray deposition and transfer printing. *Carbon*, *61*, 72–79.

[27]. **Park, J., and Hammond, P. T.** (2004). Multilayer Transfer Printing for Polyelectrolyte Multilayer Patterning: Direct Transfer of Layer-by-Layer Assembled Micropatterned Thin Films. *Advanced Materials*, *16*, 520–525.

[28]. **Basarir, F.** (2012). Fabrication of Gold Patterns via Multilayer Transfer Printing and Electroless Plating. *ACS Applied Materials and Interfaces*, *4*, 1324–1329.

[29]. **Cebeci, F. Ç., Schmidt, D. J., and Hammond, P. T.** (2014). Multilayer Transfer Printing of Electroactive Thin Film Composites. *ACS Applied Materials and Interfaces*, *6*, 20519–20523.

[30]. **Karatepe, N., and Yuca, N.** (2011). Hydrogen adsorption on carbon nanotubes purified by different methods. *International Journal of Hydrogen Energy*, *36*, 11467–11473.

[31]. **Lee, S. W., Kim, B.-S., Chen, S., Shao-Horn, Y., and Hammond, P. T.** (2009). Layer-by-Layer Assembly of All Carbon Nanotube Ultrathin Films for Electrochemical Applications. *Journal of the American Chemical Society*, *131*, 671–679.

[32]. **Zang, Z., Hu, Z., Li, Z., He, Q., and Chang, X.** (2009). Synthesis, characterization and application of ethylenediamine-modified multiwalled carbon nanotubes for selective solid-phase extraction and preconcentration of metal ions. *Journal of Hazardous Materials*,

172, 958–963.

[33]. **Ramanathan, T., Fisher, F. T., Ruoff, R. S., and Brinson, L. C.** (2005). Amino-Functionalized Carbon Nanotubes for Binding to Polymers and Biological Systems. *Chemistry of Materials*, *17*, 1290–1295.

[34]. **Wengeler, L.** (2014). *Coating and drying processes for functional films in polymer solar cells - from laboratory to pilot scale*. KIT Scientific Publishing. Retrieved from https://books.google.com.tr/books?id=57mYAwAAQBAJ

[35]. **Hunter, R. J., Ottewill, R. H., and Rowell, R. L.** (2013). *Zeta Potential in Colloid Science: Principles and Applications*. Elsevier Science. Retrieved from https://books.google.com.tr/books?id=9I3-BAAAQBAJ

[36]. **Tantang, H., Ong, J. Y., Loh, C. L., Dong, X., Chen, P., Chen, Y… Li, L.-J.** (2009). Using oxidation to increase the electrical conductivity of carbon nanotube electrodes. *Carbon*, *47*, 1867–1870.

[37]. **Graupner, R., Abraham, J., Vencelová, A., Seyller, T., Hennrich, F., Kappes, M. M… Ley, L.** (2003). Doping of single-walled carbon nanotube bundles by Brønsted acids. *Phys. Chem. Chem. Phys.*, *5*, 5472–5476.

[38]. **Geng, H.-Z., Kim, K. K., Song, C., Xuyen, N. T., Kim, S. M., Park, K. A… Lee, Y. H.** (2008). Doping and de-doping of carbon nanotube transparent conducting films by dispersant and chemical treatment. *J. Mater. Chem.*, *18*, 1261–1266.

[39]. **Manivannan, S., Ryu, J. H., Jang, J., and Park, K. C.** (2010). Fabrication and effect of post treatment on flexible single-walled carbon nanotube films. *Journal of Materials Science: Materials in Electronics*, *21*, 595–602.

[40]. **Khalid, A., Al-Juhani, A. A., Al-Hamouz, O. C., Laoui, T., Khan, Z., and Atieh, M. A.** (2015). Preparation and properties of nanocomposite polysulfone/multi-walled carbon nanotubes membranes for desalination. *Desalination*, *367*, 134–144.

[41]. **Matsumoto, K., Takahashi, T., Ishil, S., and Jikei, M.** (2015). Investigation of Dispersibility of Multi-Walled Carbon Nanotubes Using Polysulfones with Various Structures. *International Journal of the Society of Materials Engineering for Resources*, *20*, 77–81.

[42]. **Tian, Y., Park, J. G., Cheng, Q., Liang, Z., Zhang, C., and Wang, B.** (2009). The fabrication of single-walled carbon nanotube/polyelectrolyte multilayer composites by layer-by-layer assembly and magnetic field assisted alignment. *Nanotechnology*, *20*, 335601.

[43]. **Haacke, G.** (1976). New figure of merit for transparent conductors. *Journal of Applied Physics*, *47*, 4086–4089.

[44]. **Kalita, G., Matsushima, M., Uchida, H., Wakita, K., and Umeno, M.** (2010). Graphene constructed carbon thin films as transparent electrodes for solar cell applications. *J. Mater. Chem.*, *20*, 9713–9717.

[45]. **Hecht, D. S., Hu, L., and Irvin, G.** (2011). Emerging Transparent Electrodes Based on Thin Films of Carbon Nanotubes, Graphene, and Metallic Nanostructures. *Advanced Materials*, *23*, 1482–1513.

[46]. **Cheng, T., Zhang, Y.-Z., Lai, W.-Y., Chen, Y., Zeng, W.-J., and Huang, W.** (2014). High-performance stretchable transparent electrodes based on silver nanowires synthesized via an eco-friendly halogen-free method. *J. Mater. Chem. C*, *2*, 10369–10376.

[47]. **Rathmell, A. R., Bergin, S. M., Hua, Y.-L., Li, Z.-Y., and Wiley, B. J.** (2010). The Growth Mechanism of Copper Nanowires and Their Properties in Flexible, Transparent Conducting Films. *Advanced Materials*, *22*, 3558–3563.

[48]. **Kędzierski, K., Rytel, K., Majchrzycki, Ł., and Wróbel, D.** (2015). Conductive and transparent films of oriented multi-walled carbon nanotubes by Langmuir–Schaefer method. *Thin Solid Films*, *589*, 701–706.

[49]. **Fan, X., Wang, J., Wang, H., Liu, X., and Wang, H.** (2015). Bendable ITO-free Organic Solar Cells with Highly Conductive and Flexible PEDOT:PSS Electrodes on Plastic Substrates. *ACS Applied Materials and Interfaces*, *7*, 16287–16295.

[50]. **Madaria, A. R., Kumar, A., and Zhou, C.** (2011). Large scale, highly conductive and patterned transparent films of silver nanowires on arbitrary substrates and their application in touch screens. *Nanotechnology*, *22*, 245201.

[51]. **Lu, Y. C., and Chou, K. S.** (2010). Tailoring of silver wires and their performance as transparent conductive coatings. *Nanotechnology*, *21*, 215707.

[52]. **De, S., Higgins, T. M., Lyons, P. E., Doherty, E. M., Nirmalraj, P. N., Blau, W. J… Coleman, J. N.** (2009). Silver Nanowire Networks as Flexible, Transparent, Conducting Films: Extremely High DC to Optical Conductivity Ratios. *ACS Nano*, *3*, 1767–1774.

[53]. **Miller, M. S., O'Kane, J. C., Niec, A., Carmichael, R. S., and Carmichael, T. B.** (2013). Silver Nanowire/Optical Adhesive Coatings as Transparent Electrodes for Flexible Electronics. *ACS Applied*

Materials and Interfaces, *5*, 10165–10172.

[54]. **Jiu, J., Araki, T., Wang, J., Nogi, M., Sugahara, T., Nagao, S… Shinozaki, K.** (2014). Facile synthesis of very-long silver nanowires for transparent electrodes. *J. Mater. Chem. A*, *2*, 6326–6330.

[55]. **Yu, Z., Li, L., Zhang, Q., Hu, W., and Pei, Q.** (2011). Silver Nanowire-Polymer Composite Electrodes for Efficient Polymer Solar Cells. *Advanced Materials*, *23*, 4453–4457.

[56]. **Scardaci, V., Coull, R., Lyons, P. E., Rickard, D., and Coleman, J. N.** (2011). Spray Deposition of Highly Transparent, Low-Resistance Networks of Silver Nanowires over Large Areas. *Small*, *7*, 2621–2628.

[57]. **Lim, J.-W., Cho, D.-Y., Jihoon-Kim, Na, S.-I., and Kim, H.-K.** (2012). Simple brush-painting of flexible and transparent Ag nanowire network electrodes as an alternative ITO anode for cost-efficient flexible organic solar cells. *Solar Energy Materials and Solar Cells*, *107*, 348–354.

[58]. **Chen, S., Song, L., Tao, Z., Shao, X., Huang, Y., Cui, Q., and Guo, X.** (2014). Neutral-pH PEDOT:PSS as over-coating layer for stable silver nanowire flexible transparent conductive films. *Organic Electronics*, *15*, 3654–3659.

[59]. **Ye, S., Rathmell, A. R., Chen, Z., Stewart, I. E., and Wiley, B. J.** (2014). Metal nanowire networks: The next generation of transparent conductors. *Advanced Materials*, *26*, 6670–6687.

[60]. **Zabet-Khosousi, A., and Dhirani, A.-A.** (2008). Charge Transport in Nanoparticle Assemblies. *Chemical Reviews*, *108*, 4072–4124.

[61]. **Fujita, S., and Shiratori, S.** (2005). The initial growth of ultra-thin films fabricated by a weak polyelectrolyte layer-by-layer adsorption process. *Nanotechnology*, *16*, 1821–1827.

[62]. **Baba, A., Park, M.-K., Advincula, R. C., and Knoll, W.** (2002). Simultaneous Surface Plasmon Optical and Electrochemical Investigation of Layer-by-Layer Self-Assembled Conducting Ultrathin Polymer Films. *Langmuir*, *18*, 4648–4652.

[63]. **Lee, D. W., Hong, T.-K., Kang, D., Lee, J., Heo, M., Kim, J. Y… Shin, H. S.** (2011). Highly controllable transparent and conducting thin films using layer-by-layer assembly of oppositely charged reduced graphene oxides. *J. Mater. Chem.*, *21*, 3438–3442.

[64]. **Lu, L.-P., Wang, S.-Q., and Lin, X.-Q.** (2004). Fabrication of layer-by-layer deposited multilayer films containing DNA and gold nanoparticle for norepinephrine biosensor. *Analytica Chimica Acta*, *519*, 161–166.

[65]. **Zhao, S., Zhang, K., An, J., Sun, Y., and Sun, C.** (2006). Synthesis and layer-by-layer self-assembly of silver nanoparticles capped by mercaptosulfonic acid. *Materials Letters*, *60*, 1215–1218.

[66]. **Li, S.-M., Wang, Y.-S., Hsiao, S.-T., Liao, W.-H., Lin, C.-W., Yang, S.-Y… Hu, C.-C.** (2015). Fabrication of a silver nanowire-reduced graphene oxide-based electrochemical biosensor and its enhanced sensitivity in the simultaneous determination of ascorbic acid{,} dopamine{,} and uric acid. *J. Mater. Chem. C*, *3*, 9444–9453.

[67]. **Cağlayan, M. O., Sayar, F., Demirel, G., Garipcan, B., Otman, B., Celen, B., and Pişkin, E.** (2009). Stepwise formation approach to improve ellipsometric biosensor response. *Nanomedicine : Nanotechnology, Biology, and Medicine*, *5*, 152—161.

[68]. **Love, J. C., Estroff, L. A., Kriebel, J. K., Nuzzo, R. G., and Whitesides, G. M.** (2005). Self-Assembled Monolayers of Thiolates on Metals as a Form of Nanotechnology. *Chemical Reviews*, *105*, 1103–1170.

[69]. **Jiang, X., Yang, M., Meng, Y., Jiang, W., and Zhan, J.** (2013). Cysteamine-Modified Silver Nanoparticle Aggregates for Quantitative SERS Sensing of Pentachlorophenol with a Portable Raman Spectrometer. *ACS Applied Materials and Interfaces*, *5*, 6902–6908.

[70]. **Dong, T.-Y., Chen, W.-T., Wang, C.-W., Chen, C.-P., Chen, C.-N., Lin, M.-C… Kao, T.-H.** (2009). One-step synthesis of uniform silver nanoparticles capped by saturated decanoate: direct spray printing ink to form metallic silver films. *Phys. Chem. Chem. Phys.*, *11*, 6269–6275.

[71]. **Tan, L., Wan, A., and Li, H.** (2013). Conjugating S-Nitrosothiols with Glutathiose Stabilized Silver Sulfide Quantum Dots for Controlled Nitric Oxide Release and Near-Infrared Fluorescence Imaging. *ACS Applied Materials and Interfaces*, *5*, 11163–11171.

[72]. **Bayram, S., Zahr, O. K., and Blum, A. S.** (2015). Short ligands offer long-term water stability and plasmon tunability for silver nanoparticles. *RSC Adv.*, *5*, 6553–6559.

[73]. **Ding, H., Wei, J.-S., and Xiong, H.-M.** (2014). Nitrogen and sulfur co-doped carbon dots with strong blue luminescence. *Nanoscale*, *6*, 13817–13823.

[74]. **Sharon, M.** (2015). Surface Orchestration of Gold Nanoparticles Using Cysteamine as Linker and Folate as Navigating Molecule for Synaphic Delivery of Doxorubicin. *Journal of Nanomedicine Research*, *1*, 1–7.

[75]. **Zhao, T., Zhang, C., Du, Z., Li, H., and Zou, W.** (2015). Functionalization of

AgNWs with amino groups and their application in an epoxy matrix for antistatic and thermally conductive nanocomposites. *RSC Adv.*, *5*, 91516–91523.

[76]. **Dhar, N., Akhlaghi, S. P., and Tam, K. C.** (2012). Biodegradable and biocompatible polyampholyte microgels derived from chitosan, carboxymethyl cellulose and modified methyl cellulose. *Carbohydrate Polymers*, *87*, 101–109.

[77]. **Tang, M., Dou, H., and Sun, K.** (2006). One-step synthesis of dextran-based stable nanoparticles assisted by self-assembly. *Polymer*, *47*, 728–734.

[78]. **Everett, D. H.** (1988). *Basic Principles of Colloid Science*. The Royal Society of Chemistry.

[79]. **Chen, T.-G., Huang, B.-Y., Liu, H.-W., Huang, Y.-Y., Pan, H.-T., Meng, H.-F., and Yu, P.** (2012). Flexible Silver Nanowire Meshes for High-Efficiency Microtextured Organic-Silicon Hybrid Photovoltaics. *ACS Applied Materials and Interfaces*, *4*, 6857–6864.

[80]. **Lee, J. Y., Connor, S. T., Cui, Y., and Peumans, P.** (2008). Solution-processed metal nanowire mesh transparent electrodes. *Nano Letters*, *8*, 689–692.

[81]. **Tokuno, T., Nogi, M., Jiu, J., Sugahara, T., and Suganuma, K.** (2012). Transparent Electrodes Fabricated via the Self-Assembly of Silver Nanowires Using a Bubble Template. *Langmuir*, *28*, 9298–9302.

[82]. **Song, T.-B., Rim, Y. S., Liu, F., Bob, B., Ye, S., Hsieh, Y.-T., and Yang, Y.** (2015). Highly Robust Silver Nanowire Network for Transparent Electrode. *ACS Applied Materials and Interfaces*, *7*, 24601–24607.

[83]. **Sui, D., Huang, Y., Huang, L., Liang, J., Ma, Y., and Chen, Y.** (2011). Flexible and Transparent Electrothermal Film Heaters Based on Graphene Materials. *Small*, *7*, 3186–3192.

[84]. **Lan, W., Chen, Y., Yang, Z., Han, W., Zhou, J., Zhang, Y… Xie, E.** (2017). Ultraflexible Transparent Film Heater Made of Ag Nanowire/PVA Composite for Rapid-Response Thermotherapy Pads. *ACS Applied Materials and Interfaces*, *9*, 6644–6651.

[85]. **Wang, P.-H., Chen, S.-P., Su, C.-H., and Liao, Y.-C.** (2015). Direct printed silver nanowire thin film patterns for flexible transparent heaters with temperature gradients. *RSC Adv.*, *5*, 98412–98418.

[86]. **Lin, S.-Y., Zhang, T.-Y., Lu, Q., Wang, D.-Y., Yang, Y., Wu, X.-M., and Ren, T.-L.** (2017). High-performance graphene-based flexible heater for wearable applications. *RSC Advances*, *7*, 27001–27006.

[87]. **Celle, C., Mayousse, C., Moreau, E., Basti, H., Carella, A., and Simonato, J. P.** (2012). Highly flexible transparent film heaters based on random networks of silver nanowires. *Nano Research*, *5*, 427–433.

[88]. **Li, P., Ma, J. G., Xu, H. Y., Lin, D., Xue, X. D., Yan, X. Z… Liu, Y. C.** (2016). Flexible transparent heaters based on silver nanotrough meshes. *Journal of Alloys and Compounds*, *664*, 764–769.

[89]. **Kang, J., Kim, H., Kim, K. S., Lee, S. K., Bae, S., Ahn, J. H… Hong, B. H.** (2011). High-performance graphene-based transparent flexible heaters. *Nano Letters*, *11*, 5154–5158.

[90]. **Tugba Camic, B., Oytun, F., Hasan Aslan, M., Jeong Shin, H., Choi, H., and Basarir, F.** (2017). Fabrication of a transparent conducting electrode based on graphene/silver nanowires via layer-by-layer method for organic photovoltaic devices. *Journal of Colloid and Interface Science*, *505*, 79–86.

[91]. **Yang, H., Chen, T., Wang, H., Bai, S., and Guo, X.** (2018). One-pot rapid synthesis of high aspect ratio silver nanowires for transparent conductive electrodes. *Materials Research Bulletin*, *102*, 79–85.

[92]. **Oytun, F., Dizman, C., Karatepe, N., Alpturk, O., and Basarir, F.** (2017). Preparation of transparent conducting electrode on polysulfone film via multilayer transfer of layer-by-layer assembled carbon nanotubes. *Thin Solid Films*, *625*, 168–176.

[93]. **Kim, C., An, H., Jung, A., and Yeom, B.** (2017). Vortex-assisted layer-by-layer assembly of silver nanowire thin films for flexible and transparent conductive electrodes. *Journal of Colloid and Interface Science*, *493*, 371–377.

[94]. **Kim, D., Zhu, L., Jeong, D.-J., Chun, K., Bang, Y.-Y., Kim, S.-R… Oh, S.-K.** (2013). Transparent flexible heater based on hybrid of carbon nanotubes and silver nanowires. *Carbon*, *63*, 530–536.

[95]. **Kim, T., Kim, Y. W., Lee, H. S., Kim, H., Yang, W. S., and Suh, K. S.** (2013). Uniformly interconnected silver-nanowire networks for transparent film heaters. *Advanced Functional Materials*, *23*, 1250–1255.

[96]. **Sorel, S., Bellet, D., and Coleman, J. N.** (2014). Relationship between material properties and transparent heater performance for both bulk-like and percolative nanostructured networks. *ACS Nano*, *8*, 4805–4814.

[97]. **Ji, S., He, W., Wang, K., Ran, Y., and Ye, C.** (2014). Thermal response of transparent silver nanowire/PEDOT:PSS film heaters. *Small*, *10*, 4951–4960.

[98]. **Zhai, H., Wang, R., Wang, X., Cheng, Y., Shi, L., and Sun, J.** (2016). Transparent heaters based on highly stable Cu nanowire films. *Nano Research*, *9*, 3924–3936.

[99]. **Yoon, Y. H., Song, J. W., Kim, D., Kim, J., Park, J. K., Oh, S. K., and Han, C. S.** (2007). Transparent film heater using single-walled carbon nanotubes. *Advanced Materials*, *19*, 4284–4287.

[100]. **Jang, H.-S., Jeon, S. K., and Nahm, S. H.** (2011). The manufacture of a transparent film heater by spinning multi-walled carbon nanotubes. *Carbon*, *49*, 111–116.

[101]. **Oytun, F., Kara, V., Alpturk, O., and Basarir, F.** (2017). Fabrication of solution-processable, highly transparent and conductive electrodes via layer-by-layer assembly of functional silver nanowires. *Thin Solid Films*, *636*, 40–47.

[102]. **Patel, D. B., Patel, M., Chauhan, K. R., Kim, J., Oh, M. S., and Kim, J.-W.** (2018). High-performing flexible and transparent photodetector by using silver nanowire-networks. *Materials Research Bulletin*, *97*, 244–250.

[103]. **Li, J., Liang, J., Jian, X., Hu, W., Li, J., and Pei, Q.** (2014). A flexible and transparent thin film heater based on a silver nanowire/heat-resistant polymer composite. *Macromolecular Materials and Engineering*.

[104]. **Yu, Z., Zhang, Q., Li, L., Chen, Q., Niu, X., Liu, J., and Pei, Q.** (2011). Highly flexible silver nanowire electrodes for shape-memory polymer light-emitting diodes. *Advanced Materials*, *23*, 664–668.

[105]. **Choi, D. Y., Kang, H. W., Sung, H. J., and Kim, S. S.** (2013). Annealing-free, flexible silver nanowire-polymer composite electrodes via a continuous two-step spray-coating method. *Nanoscale*, *5*, 977–983.

[106]. **Song, M., You, D. S., Lim, K., Park, S., Jung, S., Kim, C. S… Kang, J. W.** (2013). Highly efficient and bendable organic solar cells with solution-processed silver nanowire electrodes. *Advanced Functional Materials*, *23*, 4177–4184.

[107]. **Langley, D., Giusti, G., Mayousse, C., Celle, C., Bellet, D., and Simonato, J. P.** (2013). Flexible transparent conductive materials based on silver nanowire networks: A review. *Nanotechnology*, *24*.

[108]. **Richardson, J. J., Cui, J., Björnmalm, M., Braunger, J. A., Ejima, H., and Caruso, F.** (2016). Innovation in Layer-by-Layer Assembly. *Chemical Reviews*, *116*, 14828–14867.

[109]. **Rydzek, G., Ji, Q., Li, M., Schaaf, P., Hill, J. P., Boulmedais, F., and Ariga, K.** (2015). Electrochemical nanoarchitectonics and layer-by-layer assembly: From basics to future. *Nano Today*, *10*, 138–167.

[110]. **Xiao, F. X., Pagliaro, M., Xu, Y. J., and Liu, B.** (2016). Layer-by-layer assembly of versatile nanoarchitectures with diverse dimensionality: A new perspective for rational construction of multilayer assemblies. *Chemical Society Reviews*.

[111]. **Richardson, J. J., Björnmalm, M., and Caruso, F.** (2015). Technology-driven layer-by-layer assembly of nanofilms. *Science*.

[112]. **Guo, R., Jiao, T., Li, R., Chen, Y., Guo, W., Zhang, L… Peng, Q.** (2018). Sandwiched Fe3O4/Carboxylate Graphene Oxide Nanostructures Constructed by Layer-by-Layer Assembly for Highly Efficient and Magnetically Recyclable Dye Removal. *ACS Sustainable Chemistry and Engineering*, *6*, 1279–1288.

[113]. **Zhao, M., Meng, L., Ma, L., Ma, L., Yang, X., Huang, Y… Guo, Z.** (2018). Layer-by-layer grafting CNTs onto carbon fibers surface for enhancing the interfacial properties of epoxy resin composites. *Composites Science and Technology*, *154*, 28–36.

[114]. **Ratanavaraporn, J., Chuma, N., Kanokpanont, S., and Damrongsakkul, S.** (2019). Beads fabricated from alginate, hyaluronic acid, and gelatin using ionic crosslinking and layer-by-layer coating techniques for controlled release of gentamicin. *Journal of Applied Polymer Science*, *136*, 46893.

[115]. **Sedighi, M., Rahimi, F., Rezayan, A. H., Shahbazi, M.-A., Witzigmann, D., and Huwyler, J.** (2018). Combined cerium oxide nanocapping and layer-by-layer coating of porous silicon containers for controlled drug release. *Journal of Materials Science*, *53*, 14975–14988.

[116]. **Liu, J., Chiam, S. Y., Pan, J., Wong, L. M., Li, S. F. Y., and Ren, Y.** (2018). Solution layer-by-layer uniform thin film dip coating of nickel hydroxide and metal incorporated nickel hydroxide and its improved electrochromic performance. *Solar Energy Materials and Solar Cells*, *185*, 318–324.

[117]. **Zhang, X., Yan, X., Chen, J., and Zhao, J.** (2014). Large-size graphene microsheets as a protective layer for transparent conductive silver nanowire film heaters. *Carbon*, *69*, 437–443.

[118]. **Hong, C.-H., Oh, S. K., Kim, T. K., Cha, Y.-J., Kwak, J. S., Shin, J.-H… Cheong, W.-S.** (2015). Electron beam irradiated silver nanowires for a highly transparent heater. *Scientific Reports*, *5*, 17716.

[119]. **Cheong, H.-G., Kim, J.-H., Song, J.-H., Jeong, U., and Park, J.-W.** (2015). Highly flexible transparent thin film heaters based on silver nanowires and aluminum zinc oxides. *Thin Solid Films*, *589*, 633–641.

CURRICULUM VITAE

Name Surname: Faruk OYTUN

Place and Date of Birth: Çanakkale-1989

E-Mail: oytunfaruk@gmail.com

University and College Degrees Obtained:

2013 – 2019 Philosophy of Doctorate

Chemistry, Istanbul Technical University, Graduate School of Science Engineering and Technology

2011 – 2013 Master of Science

Chemistry, Istanbul Technical University, Graduate School of Science Engineering and Technology

2006 – 2010 Bachelor of Science

Chemistry, Faculty of Arts and Science, Pamukkale University

Professional Experience and Awards:

2018 – 20.. Formulation Development Scientist, VSY Biotechnology

2017 - 2018 Research and Development Manager, ARES R&D Chemistry Inc

2014 - 2014 Visiting Researcher, Gwangju Institute of Science and Technology (GIST)

2013 - 2017 Ph.D. Research Fellowship, Scientific and Technological Research Council of Turkey (TUBITAK)

Publications from thesis:

- **Oytun F.,** Dizman C., Karatepe N., Alpturk O., and Basarir F., Preparation of transparent conducting electrode on polysulfone film via multilayer transfer of layer-by-layer assembled carbon nanotubes. *Thin Solid Films*, 2017, 625, 168-176.
- **Oytun F.,** Kara V., Alpturk O. and Basarir F., Fabrication of solution-processable, highly transparent and conductive electrodes via layer-by-layer assembly of functional silver nanowires. *Thin Solid Films*, 2017, 636, 40-47
- **Oytun F.,** Alpturk O. and Basarir F., Coupling layer-by-layer assembly and multilayer transfer to fabricate flexible transparent film heater, *Materials Research Bulletin*, 2019, 112, 53-60.

Other Publications:

- Camic B.T., **Oytun F.,** Aslan M.H. Shin H.J. Choi H. Basarir F., Fabrication of a transparent conducting electrode based on graphene/silver nanowires via layer-by-layer method for organic photovoltaic devices, *Journal of Colloid and Interface Science*, 2017, 505, 79-86.
- Altinkok C., **Oytun F.,** Basarir F., Tasdelen M.A., Cysteamine-functionalized silver nanowires as hydrogen donor for type II photopolymerization, *Journal of Photochemistry and Photobiology A: Chemistry*, 2017, 346, 479-484.
- Basarir F., Irani F.S., Kosemen A., Camic B.T., **Oytun F.,** Tunaboylu B., Shin H.J., Nam K.Y., Choi H., Recent progresses on solution-processed silver nanowire based transparent conducting electrodes for organic solar cells, *Materials Today Chemistry*, 2017, 3, 60-72.
- Kahveci M.K., **Oytun F.,** Yagci Y., Influence of type of zinc salts on photoinitiated living cationic polymerization of vinyl ethers, *Polymer*, 2013, 54, 4798-4801.
- **Oytun F.,** Kahveci M.K., Yagci Y., Sugar overcomes oxygen inhibition in photoinitiated free radical polymerization**,** *Journal of Polymer Science Part A: Polymer Chemistry*, 2013, 51, 1685-1689.